PREPRINT UCRL- 81699 Rev. 1

Lawrence Livermore Laboratory

SPATIAL DISTRIBUTION OF PLASMA IN A TRANSVERSE-DISCHARGE, SUPERSONIC NITROGEN STREAM

M. Garcia

CIRCULATION COPY
SUBJECT TO RECALL
IN TWO WEEKS

June 7, 1979

This paper was prepared for submittal to: Journal of Applied Physics.

This is a preprint of a paper intended for publication in a journal or proceedings. Since changes may be made before publication, this preprint is made available with the understanding that it will not be cited or reproduced without the permission of the author.

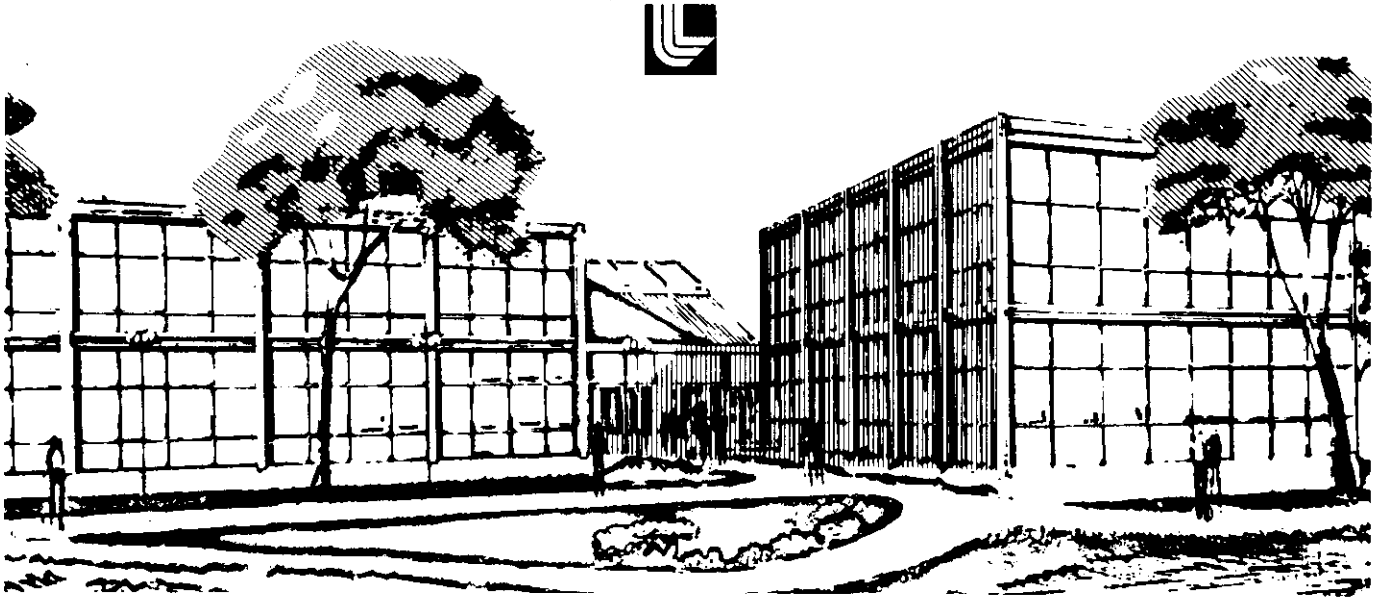

DISCLAIMER

This document was prepared as an account of work sponsored by an agency of the United States Government. Neither the United States Government nor the University of California nor any of their employees, makes any warranty, express or implied, or assumes any legal liability or responsibility for the accuracy, completeness, or usefulness of any information, apparatus, product, or process disclosed, or represents that its use would not infringe privately owned rights. Reference herein to any specific commercial product, process, or service by trade name, trademark, manufacturer, or otherwise, does not necessarily constitute or imply its endorsement, recommendation, or favoring by the United States Government or the University of California. The views and opinions of authors expressed herein do not necessarily state or reflect those of the United States Government or the University of California, and shall not be used for advertising or product endorsement purposes.

This report has been reproduced
directly from the best available copy.

Available to DOE and DOE contractors from the
Office of Scientific and Technical Information
P.O. Box 62, Oak Ridge, TN 37831
Prices available from (615) 576-8401, FTS 626-8401

Available to the public from the
National Technical Information Service
U.S. Department of Commerce
5285 Port Royal Rd.,
Springfield, VA 22161

Work performed under the auspices of the U.S. Department of Energy by Lawrence Livermore National Laboratory under Contract W-7405-ENG-48.

SPATIAL DISTRIBUTION OF PLASMA IN A TRANSVERSE-DISCHARGE, SUPERSONIC NITROGEN STREAM

M. Garcia

Lawrence Livermore Laboratory, University of California

Livermore, California 94550

ABSTRACT

Experimental and theoretical studies were conducted on plasma in a supersonic channel containing a transverse plate discharge, and localized pin discharge ionizers. The goal was to determine the mechanism by which the plasma was created and distributed in such a discharge channel, where a nitrogen flow and both discharges operated continuously. Spatially resolved measurements of neutral density ($N \approx 10^{18}$ cm^{-3}), flow velocity ($\underset{\sim}{u} \approx 540$ m/s), voltage distribution between the discharge plates (voltage drop ≈ 2 kV), and plasma density distributions have allowed for the determination of such plasma properties as the ratio of electric field to total number density ($E/N \approx 10^{-16}$ $V \cdot cm^2$), the ambipolar diffusion coefficient ($D_a \approx 40$ cm^2/s at $N \approx 10^{18}$ cm^{-3}), and the average electron energy ($\varepsilon \approx 0.7$ eV). The experimentally determined

plasma density distributions are shown to be consistent with the predictions of a continuum, quasi-neutral, convection-diffusion model with pin discharge source terms. The theory presented models all the major features of the plasma flow in the discharge channel, and can be used for future design studies of potential laser devices.

PACS numbers: 52.30.+r, 52.70.Ds.

SPATIAL DISTRIBUTION OF PLASMA IN A TRANSVERSE-DISCHARGE, SUPERSONIC NITROGEN STREAM

M. Garcia[a)]

Lawrence Livermore Laboratory, University of California
Livermore, California 94550

I. INTRODUCTION

Electric discharge excitation is a commonly used mechanism in cw laser applications. For molecular lasers such as CO and CO_2, it is well-known that the desired electric field for optimum energy transfer into vibrational states is substantially below the field necessary for a self-sustained glow discharge.[1,2] This fact, coupled with the general requirement for low translational temperature,[3,4] has led to a number of different supersonic flow ionizer-sustainer devices.[5] Probably the most effective of these has been the electron beam ionizer.[6] But the complexity and size of this apparatus prompted the exploration of simpler alternatives using uv photo-ionization, rf discharges, or pin discharges as the ionization sources.[5] The simplest option is one first investigated by Blom and Hanson, called a double discharge.[7] The purpose of the research reported here was to ascertain the

process by which plasma is created and distributed in such a double discharge device, in which gas moves at supersonic speeds.

Blom and Hanson's initial results showed a promising potential outside the self-sustained mode, but they had achieved stable operation only at relatively low plasma densities, and thus at power loadings below those necessary for laser operation. To understand the basic mechanisms and possible scaling laws for the double discharge device, a larger version was constructed at Princeton University.[8] A major design feature was the accessibility to probing, which was felt to be necessary to provide a spatially resolved data base for any physical modeling of the phenomena. All measurements reported here employed N_2 as the flowing gas. (See Figs. 1 and 2.)

Section II describes the new device and reports extensive tests of its overall operating characteristics. Among the results are the voltage-current characteristics of the main discharge for several pin currents. An understanding of the mechanism by which the plasma is created at the pin discharges (within the boundary layer at the cathode), spreads to the anode, and allows passage of the main current is clearly essential to any potential extension of the operating range of the double discharge device. To provide the data necessary for the testing of any theoretical model, spatially resolved

measurements were performed at two axial positions. Pitot pressure surveys were made to determine the local flow conditions.

In Sec. III, a theoretical model of the plasma is developed, based on continuum theory and the quasi-neutral assumption. The pin discharges are modeled by sources at the location of the pins. With electron attachment and recombination neglected, a Green function solution is obtained in the simplified case where the neutral flow velocity, ambipolar diffusion coefficient D_a, and ionization coefficient are uniform.

Section IV then presents spatially resolved electrostatic probe measurements of the local floating potential and rms current under several conditions, but with only one center pin discharge in operation. This condition was felt to be the easiest to interpret and model theoretically.

Floating potential probe measurements were made at the middle and trailing windows of the device. These data show that the electric field was not constant even outside the cathode fall and anode sheath regions. Measurements of rms probe current at 200 Hz (a region of relative plasma quietness) were made by sweeping the probe between -5 V and +5 V, and reading the voltage across a calibrated resistor with a lock-in amplifier. The range of conditions was such that the rms voltage measurements directly show relative number density

values with great accuracy.[8,9] Peak density was about 3×10^9 cm^{-3}. The plasma cloud showed a relatively modest horizontal spread even 20 cm from the pin discharge, and a vertical drop-off near the cathode.

In Sec. V, theory is compared to experiment by considering relative plasma density profiles in y and z, as well as the quantity D_a. Theoretical profiles contain D_a as a parameter. For a theoretical profile that matches a probe signal profile closely, a comparison is made between the value adopted by the fit parameter D_a and the actual (locally measured) value of the ambipolar diffusion coefficient. The comparisons are generally very good in terms of the shape of the z-profiles. The "best fit" value of D_a is well within experimental accuracy of D_a as computed on the basis of nitrogen data at the experimental values of (E/N) and N. The y-profiles cannot be matched by a single delta function source solution, but they can be matched by assuming a line source (with exponentially decaying source strength) above the pin discharge. The validity of the model advanced appears to be established by the available evidence.

II. DOUBLE DISCHARGE DEVICE

A. Previous designs

To construct high power, electrically excited lasers operating off molecular vibrational-rotational bands, one must

produce in a large volume of cold gas a significant number of electrons at an (E/N) level below that needed for self-sustained glow discharge. The ideal would be a uniform volume of plasma with

$$
\begin{aligned}
N&: \quad 10^{18} \text{ to } 10^{20}\ \mathrm{cm}^{-3} \\
(n_e/N)&: \quad 10^{-7} \text{ to } 10^{-6} \\
(E/_N)&: \quad 10^{-17} \text{ to } 10^{-15}\ \mathrm{V \cdot cm}^2 \\
\varepsilon&: \quad 1 \text{ to } 2\ \mathrm{eV} \\
T&: \quad 70 \text{ to } 90\ \mathrm{K}.
\end{aligned}
$$

No static, self-sustained dc discharge has been developed which can duplicate these conditions. In a self-sustained discharge there is a coupling between the processes of electron production and electron heating. Hence, both n_e and ε cannot be specified.

The background gas in static discharges is resistively heated by current passage. Hence, it is difficult to maintain a uniform low temperature in the discharge volume by relying solely on diffusion-dominated wall cooling. As the current draw is increased in an effort to elevate n_e, local nonuniformities in energy density tend to produce instabilities which can lead to arcing.[10,11] Arcing is an anathema for laser operation as it heats the gas and collapses the plasma into a small volume.

Some of these difficulties may be relieved by relying on convective, as opposed to diffusive, cooling of the discharge volume. Large volumes of low temperature gas can be produced by a fast flow, such as a supersonic expansion. Flows help stabilize discharges by convecting out of the discharge volume any gas cells that may contain growing instabilities.[10,11] The turbulence introduced by flows enchances molecular transport, thereby reducing density nonuniformities which can be destabilizing. For these reasons, many experimenters attempted to produce stable, distributed plasmas in supersonic streams. Since they sought independent control of (E/N) and n_e, they tried to stabilize non-self-sustaining discharges by some form of auxiliary ionization. Several approaches were tried, including the use of electron beams or ultraviolet sources to pump non-self-sustaining discharges. Devices such as these which attempt to place independent controls on electron density and average energy are termed ionizer-sustainer devices. Reilly has described many of the ionizer-sustained laser experiments in his review of electric discharge laser development.[5]

One scheme that attracted attention because of its inherent simplicity and promising performance in small scale was the continuously operating double discharge device of J. H. Blom and R. K. Hanson[7] at Stanford University. Their device was a small, acrylic supersonic channel. The floor and ceiling

consisted of flush-mounted copper plate electrodes. Embedded in the grounded cathode and flush with its surface was an array of tungsten pins insulated by epoxy sleeves. Separate power supplies energized the anode plate and the pin array; the grounded cathode was common.

The primary purpose of this device was to investigate the mechanism by which a discharge can be run at an optimal (E/N) value for energy deposition in vibration, using the plate power supply to produce the desired field. Since this requires some auxiliary source of electrons to maintain the current drawn in the face of diffusion, recombination, and attachment losses, the pin discharges were provided. These pin discharges were confined entirely in the velocity boundary layer over the cathode surface.

Blom and Hanson showed that voltage changed slowly as the anode current swept over the operating range (0-0.1 up to 0-0.3 A, depending on pin current level). Higher anode voltages could be selected by decreasing the pin current level. Blom and Hanson presented anode voltage vs anode current characteristics that were flat or shallow curves.[7]

B. Construction of improved device

The electric discharge channel reported here is an enlarged version of the Blom-Hanson project. It has been used (1) to study the effect of physical scale on the electrical operating

characteristics of a device that has twice the gap, 3 times the width, and 20 times the discharge volume as the Blom-Hanson facility, and (2) to probe the flow and plasma in a spatially resolved manner (because of the larger scale) to provide some fundamental understanding of the mechanisms involved.

The discharge channel consists of a supersonic nozzle, a discharge volume, and a diffuser section coupled to a multistage ejector system. The entire assembly, except for the electrodes, is acrylic. This electrically insulates the discharge from the intake and exhaust plumbing. Figure 1 provides a schematic of the facility.

For convenience, the following coordinate system has been adopted:

x: in the direction of the flow,

y: perpendicular to the cathode surface,

z: along the cathode surface, but perpendicular to the flow.

The origin of this system is usually placed on the leading edge of the cathode surface (Fig. 2). Electrons migrate to the anode in the positive y-direction. The gas expands in the x-direction, and one sights along the z-direction when viewing the interior of the tunnel through the window ports on its side.

The nozzle has a two-dimensional, contoured design. (For construction details on all parts, see Appendix A.) In the

discharge volume behind the nozzle, a small vertical expansion helps to compensate for the effect of boundary layer growth. The electrode plates span the full width of the flow, and are flush with the tunnel floor (cathode) and ceiling (anode). Embedded in the cathode is a flush-mounted matrix of 35 tungsten pin electrodes, each with an insulator sheath. The cathode has cooling water passages milled into it between the pins and close to the flow; similar passages are milled into the acrylic piece above the anode. Such cooling prevents excessive heat from damaging the pin insulators or the surrounding plastic structure, a problem encountered by Blom and Hanson.[7]

Six circular window ports provide access to the interior of the discharge volume. A probe drive, adjustable in both the y- and z-direction, could easily replace any of these window plugs for Pitot or plasma probing.

A general circuit diagram of the double discharge channel appears in Fig. 3. The anode power supply has a rated capability of 5 kV at 1 A (dc), with a measured ripple of less than 1%. Because glow discharges of the type produced in this device are at best marginally stable,[12] one must use a series ballast resistor to provide macroscopic stability, and to limit current draw in case of an arc-over. All tests described here were made with a 1-kΩ ballast resistor.

The pin power supply offers 1.25 kV at 2.5 A (dc) with a 1% ripple. Ten parallel 3-kΩ ballast resistors each feed into separate coaxial cables. Thus one may power any 10 pins simultaneously at up to 0.25 A, or drive a single pin with up to 2.5 A. Because the cathode is at ground potential, the double discharge therefore consists quite simply of two high voltage anodes with a common cathode.

The discharge channel is a nonideal wind tunnel with a complicated flow field. Pitot pressure probes and wall static pressure taps were used to explore the interior of this flow. These experimental investigations yielded neutral density and flow velocity profiles between the discharge plates (see Figs. 4 and 5). It was also found that because of the low power density of the discharge, no flow heating with attendant property changes would occur. This information on spatially resolved density N and on velocity $\underset{\sim}{u}$ was essential for later determining spatially varying plasma properties (E/N, D_a, μ_+, α). The details of neutral flow field experiments, as well as sample data, are reported in Ref. 8.

C. Operation

A plasma is produced in the discharge channel by first establishing a flow, then energizing the pins, and then activating the anode plate. The bright blue[13] pin plasma plumes are sharply swept back by the flow at lower pin currents

(0 to 100 mA). These plumes are not much wider than the pins producing them. Only a few millimetres high, they extend from 1 to 2 cm downstream. As the pin current is increased, the cathode spot of the pin plasma expands in all directions. At high pin currents (> 1 A/pin) it extends up to 2.5 cm both laterally and upstream, and 5 cm downstream. The most intense luminescence in the plume is near the pin itself and directly downstream from it.

As plate voltage rises, the plasma plume extends rapidly downstream until it reaches the end of the electrodes. This translucent blue cloud can be quite narrow if produced by a solitary pin near the tunnel centerline, even for high pin currents where an extended pin plasma cloud exists near the upstream end of the discharge volume. Increases in anode current (or voltage) always produce increased intensity, with small amounts of lateral spreading.

With the outermost pins (0.66 cm from the sidewall) activated, there is a strong tendency for arcing to occur between the plates in the sidewall boundary layers. Arc filaments emanate from the electrode-sidewall corners. This condition destroys glass and acrylic; hence, it was studiously avoided. With no pins activated at all it was impossible to produce any plasma. So the pins are quite clearly needed to maintain the discharge.

D. Voltage-current characteristics

Anode voltage-current characteristics, parameterized by pin current, were quite similar to those seen before at Stanford.[7] They exhibited the same trends with respect to changes in external parameters (see Fig. 6). With a stable distributed glow situated in the discharge volume, an increase in stagnation pressure at a constant pin current level causes the anode voltage to rise in order to maintain the same flow of anode current. Decreasing the pin current has an effect analogous to increasing the stagnation pressure. The discharge operation becomes unstable if the decrease in pin current or the increase in stagnation pressure is too great.

Between stable and unstable operation lies a transition region. It is characterized by anode voltage oscillations whose period equals 1 discharge-volume flow time (1 ms) and whose amplitude grows with increasing anode current. In the region of complete instability, single pinkish-orange[14] arcs appear, which travel one at a time with the flow at 540 m/s through the discharge volume. Blom and Hanson[7] also found anode voltage oscillations during such unstable operation, with a period equal to the discharge-volume flow time. The transition between stable and unstable operation, as well as qualitative and quantitative information on the arcing phenomena, are discussed at length by Garcia.[8]

III. THEORETICAL MODEL OF DOUBLE DISCHARGE PLASMA

This section presents a general formulation of the equations governing the plasma flow. First, it reviews assumptions made about the composition of the flow. Then both the species continuity and momentum equations are presented. These are combined, using the assumption of quasi-neutrality, into a single equation for the density of plasma in the discharge volume. I begin with the simplest possible case: a plasma whose properties are constant in space, so that for fixed (E/N) and N everywhere, the ambipolar diffusion coefficient and ionization rate coefficient are constant. I then give the solution of the derived equation for the case of a delta function plasma source term (modelling a pin electrode). This solution is in fact a Green function. Clearly, the possibility exists for determining the plasma density for more complex, spatially distributed sources by using the Green function solution.

A. Assumptions

First, I assume that the discharge channel contains a steady state flow: a mulitcomponent conducting medium that is spatially inhomogeneous. Second, for electron energy near 1 eV and density about 10^{10} cm^{-3}, the Debye length is of the order of 10^{-3} cm. Because this length is smaller than any flow field length scale, we may assume a continuum or fluid

model to describe the major features of the plasma density distribution.

Under such a model, the conservation equation of particle density for each species has the form

$$\underset{\sim}{\nabla} \cdot \underset{\sim}{\Gamma}_s = \underset{\sim}{\nabla} \cdot (n_s \underset{\sim}{v}_s) = S_s \quad , \tag{1}$$

where $\underset{\sim}{\Gamma}_s$, n_s, $\underset{\sim}{v}_s$, and S_s are the flux vector, number density, velocity and source term of species S. The ionization fraction (n_e/N) of the plasma in the double discharge is about 10^{-8}. Because $(n_e/N) << 1$, the level of neutral particle density will be virtually unaffected by any rate of charged particle production. Hence, we assume that the conservation equations for the neutral species may be uncoupled from those for the charged particles. The neutral properties may be considered as a known quantity in the latter equations.

In gas mixtures of current interest in laser discharges the charged particles are positive and negative ions, and electrons. In the case of a nitrogen stream, negative ions are unlikely because the electron affinity for molecular nitrogen is less than zero (indicating an unstable ion). So long-lived N_2^- ions are absent.[15] The electron affinity of nitrogen atoms is near zero, and the only observation of N^- ions has

been in high energy charge transfer collisions involving N^+ ions and gas molecules.[16] This process is unlikely to occur in the present apparatus. So my fourth assumption is that one may neglect both attachment and negative ions in the nitrogen double discharge.

Because of the low ionization fraction, it is also accurate to assume that positive ions are singly charged. And finally, the small Debye length and the nature of the plasma composition make quasi-neutrality,

$$n = (n_e \approx n_+) \quad , \tag{2}$$

another good assumption.

Hence, the analysis below relies on the following assumptions:

(a) steady state flow,

(b) continuum model,

(c) uncoupled neutral flow,

(d) negligible attachment and no negative ions in nitrogen,

(e) singly charged positive ions,

(f) quasi-neutrality.

It will include a treatment of ambipolar diffusion, convection, and volumetric production of plasma in the discharge.

B. Plasma equations

The charged particle conservation equations that result from the preceding assumptions are:

$$\underset{\sim}{\nabla}\cdot\underset{\sim}{\Gamma}_e = \underset{\sim}{\nabla}\cdot(n_e\underset{\sim}{v}_e) = S \quad , \tag{3}$$

$$\underset{\sim}{\nabla}\cdot\underset{\sim}{\Gamma}_+ = \underset{\sim}{\nabla}\cdot(n_+v_+) = S \quad , \tag{4}$$

where the rates of electron and ion production are equal. The momentum equations for electrons and ions are:

$$\underset{\sim}{\Gamma}_e = n_e\underset{\sim}{v}_e = -D_e\,\underset{\sim}{\nabla}n_e - \mu_e n_e\underset{\sim}{E} + n_e\underset{\sim}{u} \quad , \tag{5}$$

$$\underset{\sim}{\Gamma}_+ = n_+\underset{\sim}{v}_+ = -D_+\,\underset{\sim}{\nabla}n_+ + \mu_+ n_+\underset{\sim}{E} + n_+\underset{\sim}{u} \quad . \tag{6}$$

Here D_s and μ_s are the diffusion and mobility coefficients of species s, $\underset{\sim}{u}$ is the neutral or mass average velocity and $\underset{\sim}{E}$ is the electric field.

For this problem with no magnetic fields, the only relevant electrodynamic equation is Poisson's equation:

$$\underset{\sim}{\nabla}\cdot\underset{\sim}{E} = \frac{e}{\varepsilon_o}(n_+ - n_e) \quad . \tag{7}$$

Substitution of each species momentum equation into its corresponding continuity equation produces a set of coupled partial differential equations that, in conjunction with

Poisson's equation, completely specifies all particle densities and the electric field.

Analysis of the continuum plasma flow is simplified significantly when proper use is made of quasi-neutrality.[17] An equation for the plasma density n can be derived which does not depend explicitly on the electric field.

Let

$$\underset{\sim}{\Gamma} = \underset{\sim}{\Gamma}_+ + \frac{\mu_+}{\mu_e} \underset{\sim}{\Gamma}_e \quad . \tag{8}$$

The divergence of this vector is

$$\underset{\sim}{\nabla} \cdot \underset{\sim}{\Gamma} = \underset{\sim}{\nabla} \cdot \left[\left(1 + \frac{\mu_+}{\mu_e} \right) \left(-D_a \underset{\sim}{\nabla} n + n \underset{\sim}{u} \right) \right] = \left(1 + \frac{\mu_+}{\mu_e} \right) S \quad . \tag{9}$$

Here

$$D_a = \frac{D_+ + (\mu_+/\mu_e)\, D_e}{1 + (\mu_+/\mu_e)} \quad , \tag{10}$$

which is called the ambipolar diffusion coefficient. The ratio (μ_+/μ_e) is of order $(m_e/m_+)^{\frac{1}{2}}$, which is considerably less than one. Because this ratio changes very little in the discharge volume, the equation for plasma density can be approximated by

$$\nabla \cdot \left[-D_a \underset{\sim}{\nabla} n + n \underset{\sim}{u} \right] = S \quad . \tag{11}$$

This equation for n depends on the electric field only implicitly, through D_a and S.

In order to compute the electric field, one considers current conservation.[17] The current density is:

$$J = e\left[\underset{\sim}{\Gamma}_+ - \underset{\sim}{\Gamma}_e\right] \quad . \tag{12}$$

Current conservation yields:

$$\underset{\sim}{\nabla}\cdot\underset{\sim}{J} = 0 = \underset{\sim}{\nabla}\cdot\left\{en(\mu_+ + \mu_e)\left[\frac{D_e - D_+}{\mu_e + \mu_+}\frac{\underset{\sim}{\nabla}n}{n} + \underset{\sim}{E}\right]\right\}. \tag{13}$$

The electric field can be expressed in two parts as

$$\underset{\sim}{E} = -\left(\frac{D_e - D_+}{\mu_e + \mu_+}\right)\frac{\underset{\sim}{\nabla}n}{n} + \underset{\sim}{E}_0 \quad . \tag{14}$$

The first term is the ambipolar field, which essentially maintains quasi-neutrality; the second term is the current conduction field. Substitution of the above expression for $\underset{\sim}{E}$ into Eq. ,(13) results in

$$\underset{\sim}{\nabla}\cdot\left|en(\mu_e + \mu_+)\ \underset{\sim}{E}_0\right| = \underset{\sim}{\nabla}\cdot(\sigma\underset{\sim}{E}_0) = 0 \quad , \tag{15}$$

where σ is the conductivity of the plasma.

Except for the neglect of attachment (and detachment), the treatment thus far has been independent of the nature of the

source terms. Effects such as electron impact ionization, volume recombination, and photoionization, as well as models of the pin discharge sources, can all be included in S. This procedure is good for any multicomponent, continuum plasma. However, solution of this system is not simple in situations of experimental interest.

In plasmas of the type produced by the double discharge, collisional ionization is likely to predominate over photoionization. As electron-molecule inelastic collision cross sections are generally larger than photoionization cross sections, and as low energy electrons are much more abundant than multivolt photons, the neglect of photoionization is reasonable.[18]

Under these assumptions the plasma source term becomes

$$S = \alpha n - \rho n^2 + A(\underset{\sim}{x}) \quad , \tag{16}$$

where α, ρ and $A(x)$ are the net volume ionization rate, the electron-ion recombination coefficient,[19] and the source term due to the pin discharges. Equation (11) then becomes

$$\underset{\sim}{\nabla} \cdot \left[-D_a \underset{\sim}{\nabla} n + n \underset{\sim}{u} \right] = \alpha n - \rho n^2 + A(\underset{\sim}{x}) \quad . \tag{17}$$

Together, Eqs. (15) and (17) govern plasma behavior. I assume that D_a, α, ρ, and $A(x)$ do not depend on the electric field, so

that Eqs. (15) and (17) can be uncoupled and so that only Eq. (17) need be studied to determine plasma density.

A solution to Eq. (17) exists for the case of a semi-infinite region above a cathode at $y = 0$, where u is a uniform flow parallel to this surface, D_a and α are constant, ρ is 0, and the source term is a delta function. Garcia[8] gives the details of this derivation. Briefly, the plasma density at (x, y, z) is

$$n = \left(\frac{\pi}{2}\right)^{\frac{1}{2}} \frac{A_0}{D_a} \frac{\exp\left[\frac{1}{2}k(x - x_0) - \beta r\right]}{r} \times \left[1 \mp \frac{\exp\left\{-\beta r\left[(1 + 4yy_0 r^{-2})^{\frac{1}{2}} - 1\right]\right\}}{(1 + 4yy_0 r^{-2})^{\frac{1}{2}}}\right] , \qquad (18)$$

where A_0 is the strength of source A ($cm^{-3}\ S^{-1}$) located at (x_0, y_0, z_0), $k = (u/D_a)$, $\beta = \left[(u/2D_a)^2 - (\alpha/D_a)\right]^{\frac{1}{2}}$, and r is the distance to point (x, y, z) measured from the source. The upper (negative) sign applies for zero density at the electrode surface; the lower (positive) sign applies when the normal gradient of density is zero at the cathode. Quasi-neutrality disappears within several Debye lengths of the electrode surface. Hence, the appropriate boundary conditions for the quasi-neutral problem must come either from a rigorous analysis of the nonneutral plasma flow in the electrode sheath, or from comparison with experimental measurements of plasma density.

The plasma density near the cathode is over 10 times greater than near the anode (at y_A). As a result, a semi-infinite region can be used to model the quasi-neutral flow. This simplifies the mathematics by eliminating the boundary condition at $y = y_A$.

The equation governing the behavior of the plasma density distribution is linear. Therefore, when the source term is a distribution of delta functions with strengths A_{0i} at points (x_{0i}, y_{0i}, z_{0i}) for $i = 1, 2, \ldots n$, the resultant solution is a summation of individual solutions of Eq. (18) over i. The constant density contours of the solution of Eq. (18), when a zero-density boundary condition holds at the cathode surface, are shown schematically in Fig. 7.

IV. MEASUREMENT TECHNIQUE

Using an electrostatic probe, spatially resolved measurements of plasma density n_e were made at two cross sections of the discharge channel (the center (e) and rear (f) port positions shown in Fig. 2). Two sets of data were taken at each cross section, one at P_0 = 239 kPa and one at half the neutral density level with P_0 = 120 kPa, but with the pin and plate currents unchanged. The probe was scanned vertically between the discharge plates, as well as horizontally between adjacent window ports. This yielded both vertical (y) and horizontal (z) relative plasma density profiles.

A. Probe theory

Any charged body (a probe) placed in a neutral plasma will have a nonneutral sheath surrounding it. This sheath region contains the majority of the potential drop between the probe and plasma. The probe will collect charges by accelerating toward itself, in the outer region or "edge" of the sheath, particles that bear the opposite charge. When the potential difference between the probe and plasma is greater than the average energy of electrons in the plasma, then particles at the sheath edge will not be energetic enough to counteract the potential drop and escape from the probe. When this occurs, the limitation on the amount of probe current collected is the mechanism that transports charges to the vicinity of the probe. The probe current just described is called the saturation current (electron saturation for positive potentials and ion saturation for negative potentials). Electrostatic probes actually measure current. The relationship between this probe current and plasma number density must be supplied by an analysis usually termed a probe theory. One may assume here that plasma density is linearly related to ion saturation current:

$$I_{SAT} = en_e uA \quad .$$

The quasi-neutral plasma is swept downstream at the flow velocity $\underset{\sim}{u}$, and all particles in a stream tube of

cross-sectional area A are carried into an electric sheath where they are retrieved by the probe. The sheath thickness should vary fairly slowly over the range of plasma densities encountered. Thus the area A is likely to vary little through most of the plasma cloud, and distributions of n_e can be assumed equivalent to distributions of I_{SAT}. This matter is discussed at great length by Garcia,[8] and the connection between saturation current and rms current is presented in Appendix B.

From the shapes of horizontal density profiles one can deduce the local ambipolar diffusion coefficient. This is done by fitting a curve of the type anticipated by theory to the data trace. Because the values of (E/N) and N are also known in the regions probed, the ambipolar diffusion coefficient for nitrogen can be calculated and compared with the deduced value. If the two values of this coefficient are close, then the theoretical picture can be considered generally correct. This comparison appears below, after a brief description of the experimental technique used in obtaining the data.

B. Probe design and use

The local measurements of plasma density distribution and floating potential were carried out using a single electrostatic probe. Figure 8 shows the circuit. As the plasma electrons have an energy of about 1 eV, an electric probe in the plasma

should saturate when biased by a few volts from floating potential. A measurement of this saturation current can be related to plasma density.[8]

The technique employed here was to input a 5-V, 200-Hz sine wave through a dc blocking capacitor to the probe. Circuit components were specified such that the probe-to-plasma voltage drop was practically the entire 5 V. The 200-Hz current was monitored on the low voltage side of the capacitor by measuring the differential rms voltage across a precision resistor with a lock-in amplifier (Princeton Applied Research Model HR-8).[20] The frequency of 200 Hz was chosen because the plasma, checked with a spectrum analyzer, was relatively quiet there. In the range of 100 to 300 Hz, plasma fluctuations consist of white noise 1.6 V in amplitude. The lock-in amplifier can detect a signal to better than 0.25 Hz in noise up to 1000 times stronger than the signal. High frequency probing was avoided because the magnitude of the current drawn as a result of capacitive coupling to ground was comparable to, if not larger than, the signal. The signal ranged up to 50 μA. Readings of these saturation currents (rms voltages), when plotted against position, produced relative plasma density maps.

The probe electrode was a cylinder 0.0635 cm in diameter and 0.1 to 0.16 cm long (actually, the end of a steel drill bit). The cylinder faced into the tunnel flow and was tilted slightly

downward (4°) for most tests. It was silver soldered to a stainless steel strut with diamond cross section. The strut was silver soldered to a brass tube encased in a circular acrylic sleeve. After the strut and probe electrode were coated with insulating paint (G.E. Glyptal), a probe area was established by scraping paint off the electrode tip.

Readings of rms voltage on the test resistor were taken with the facility not in operation, to determine the inherent noise level of the probe circuitry. This noise was found to consist entirely of cable capacitance and to be quite low compared to actual data levels. It was always measured before and after runs and subsequently subtracted from the signals when they were evaluated.

Over a period of about 10 s, the phenomena occurring in the discharge channel were not precisely steady. For this reason, vertical bars are plotted with each data point (e.g., Fig. 9) to record the observed minimum and maximum values of the lock-in amplifier output at the location in question. These probe response fluctuations become relatively more pronounced in regions of low plasma concentration, or near the anode. The plotted point within each vertical bar shows the most frequently observed value, while the horizontal bars indicate the probe face diameter. The figures thus show the full range of detected signals, clustered about the point of most probable value. This

data spread results from changes in tunnel conditions and it completely overshadows any error associated with the instrumentation.

The largest rms voltage that can be measured by the lock-in amplifier is 0.5 V. Data presented here (10 to 500 mV) have had the circuit noise subtracted (5 to 8 mV), and have been normalized by 500 mV. The absolute value of a voltage signal depends on the actual exposed probe area, which varies from one probe to another. So these data are for probes whose areas match as closely as possible.

Figures 9 to 13 show density profiles taken horizontally and vertically at both the center and rear window ports (P_0 = 239 kPa). The width of the plasma plume behind a single pin discharge near the cathode varies from 1 to 1.25 cm. Figure 9 is a vertical trace near the plasma cloud centerline at the center port. Figure 10 presents normalized horizontal probe signal contours corresponding to the vertical trace in Fig. 9. Figure 11 is a cross plot made from Fig. 10, and maps out the constant-signal contours in a cross section of the plasma.

Figure 12 is a vertical density profile at the rear port near the tunnel centerline (anode at 2.85 cm). Figure 13 shows a horizontal data scan for the same conditions (at 0.28 cm above the cathode). Similar data for P_0 = 120 kPa appear in Ref. 8.

Profiles of log N along the y- and z-axes exhibit two trends: (1) horizontal (z) profiles appear as parabolas with maxima near the tunnel centerline, and (2) vertical (y) profiles show a nearly linear decay from high levels at low y-values.[21] The floating potential was measured using a Keithley Model 602 electrometer and a 1-TΩ, 1000:1 Keithley voltage divider. A sample voltage profile between the discharge plates, at the center window port and for P_0 = 239 kPa, is shown in Fig. 14.

Plotted along with this floating potential profile is a least squares fit, which follows the data quite closely over most of the gap and is used in evaluating the local field and (E/N). This least squares fit is to a Gaussian curve whose maximum falls at the anode. In the top quarter of the gap height, data are extremely hard to obtain and considerably less reliable than near the cathode. Because most data points lie in the lower region, the curve fits obtain whether or not the points in the upper quarter of the gap are used. As the region of interest is in the lower three-quarters of the gap, the Gaussians fitted to the floating potential data were taken as accurate surrogates for the data points.

Profiles of (E/N) between the discharge plates can be constructed from the floating potential and the density profiles. Figure 15 contains an example, where $y/y_I = 0$ is the cathode.

V. COMPARISON OF THEORY WITH EXPERIMENT

A. Procedure

The comparison of theory with experiment is accomplished in four steps:

(i) The functional dependence of plasma density with respect to each of y and z, at any tunnel cross section, is deduced from theory.

(ii) The experimental plasma density profiles in y and z are fitted by curves of the type deduced in (i), using the method of least squares.

(iii) Specific values of a fit coefficient produced in (ii) are related to local values of the ambipolar diffusion coefficient D_a, a measurable plasma property.

(iv) A comparison is made between values of D_a obtained in (iii) and the results of direct experimental determinations of this property.

The quality of the data-theory correlation is judged by two criteria: the match between D_a values (iv), and the goodness of fit to experimental density profiles (ii).

B. Functional form of plasma density profiles

1. Theoretical y-profiles

The actual plasma source in the discharge channel is not a simple delta function. Above the cathode, near the leading edge of the discharge volume, the plasma density should be quite

low. The Debye length may be comparable to tunnel dimensions, and quasi-neutrality is unlikely to obtain. Because of the voltage drop across the discharge gap, electrons will be accelerated vertically, and will be more energetic than in quasi-neutral regions. These electrons may collisionally ionize gas molecules, effectively creating a vertical plasma source distribution. This initial distribution flows downstream and diffuses, under the influence of the electric field, into the observed plasma cloud. Were the source distribution known, it could be approximated by a series of appropriately weighted delta functions for purposes of theoretical computation. But the form of the distributed source is not known, so a simple exponential decay in y is assumed at the centerline value of z.

The source distribution used in the computations below consists of 10 points. They are spaced at (y/y_I)-intervals of 0.118 along the y-axis between 0 and 1.063. The weight W_i for location i is given by $\left(A_i / \sum_{j=1}^{10} A_j\right)$, where $A_i = \exp\left[-y_i(\mathrm{cm})/l(\mathrm{cm})\right]$.

By assuming y-distributions of source delta functions, computing the resultant plasma density function, and comparing with measurements of vertical (y) plasma profiles at different values of x, one can deduce the general shape of the actual source. The e-folding distance of 1 cm for the exponential source was determined in this fashion.

As Sec. E will show, the effect of D_a on the vertical plasma distribution at any x is negligible. Vertical plasma density profiles are the result of convection of the source profile downstream (along x). The x-variation of plasma density is of the form $\left[(\pi/2)^{\frac{1}{2}} A_0 e^{(\alpha x/u)}\right]/D_a x$ (see Eq. 19 below). Whether the exponential or the (1/x) term dominates depends on the relative magnitude of parameters α, u, and D_a.

2. Theoretical z-profiles

If one considers a (y, z) cross section directly downstream from a single delta-function source near the cathode, and if the radius of this section is significantly smaller than the distance from the source, so that

$$|x - x_0| \gg \left[(y - y_0)^2 + (z - z_0)^2\right]^{\frac{1}{2}} \quad ,$$

then the analytic expression for the plasma density in this case (Eq. 18) can be approximated by

$$n((\text{fixed } x),y,z) = \left(\frac{\pi}{2}\right)^{\frac{1}{2}} \frac{A_0}{D_a} \frac{\exp\left[(\alpha/u)\ |x - x_0|\right]}{|x - x_0|}$$

$$\times \exp\left[-\frac{1}{2}\left(\frac{k^2}{4} - \tilde{\alpha}\right)^{\frac{1}{2}} \frac{\left[\left(y - y_0\right)^2 + \left(z - z_0\right)^2\right]}{|x - x_0|}\right], \qquad (19)$$

where

$$k = (u/D_a) \text{ and } \tilde{\alpha} = (\alpha/D_a) \quad .$$

Knowledge of the velocity profiles and the ability to compute α have confirmed that $(k^2/4) \gg \tilde{\alpha}$ in most of the double discharge. Hence, the radical in the exponent of the cross-sectional variation term of Eq. (19) can be approximated by $(u/2D_a)$, and the exponent becomes

$$- \frac{u}{4D_a} \frac{\left(y - y_0\right)^2 + \left(z - z_0\right)^2}{|x - x_0|} \quad .$$

Given a horizontal (z) density profile, a least squares fit to the exponential curve

$$n = ae^{-bt}$$

can be made between n and the variable $t = \left[(y - y_0)^2 + (z - z_0)^2\right]/|x - x_0|$. The coefficient b that results is equal to $(+u/4D_a)$, and so D_a can be computed from $D_a = (u/4b)$.

If a distributed plasma source is situated between the discharge plates near the leading edge of the discharge volume, then the plasma density function would be an integral involving the Green function and the source term. Consider the case of a line source of nonuniform strength at the tunnel centerline $(z = z_0)$. As this source has no lateral variations, the

plasma density at a given cross section ($x = x_1$) far from the source can be found to have the form

$$n(x_1,y,z) = f(y)c \exp\left|d(z - z_0)^2\right| \quad ,$$

where c and d are constants.

Thus for any sufficiently distant tunnel cross section, normalized horizontal (z) density contours will be equivalent, Gaussian curves. For a line source, then, the shape (but not the magnitude) of horizontal data profiles is independent of the manner in which the strength is distributed along the length of the source.

In deducing ambipolar diffusion coefficients from data, only the shape and not the magnitude of the profiles is required. Therefore, it is entirely correct and appropriate to use the approximate form of the single-source point solution (just developed as Eq. (19)) in analyzing horizontal data profiles, even though a line source may be acting.

C. Fitting data with predicted profiles

Figures 16 and 17 show computed, normalized, vertical (y) and horizontal (z) plasma density profiles. They were computed using D_a and α values from the region near $(y/y_I) = 0.2$, where D_a hardly varies with respect to y (see Fig. 18). The normalization constants used here are the maximum cross section

plasma densities, and all computed profiles are for unit source flux. The boundary condition at the cathode surface was taken to be a zero vertical gradient of plasma density.[22] The normalized vertical density profile produced in this way matches the experiment quite well, and varies little with large changes in D_a or u (see Fig. 16).

In Fig. 19 computed, normalized horizontal profiles are compared to normalized experimental data. Some data have been reflected about the profile centerline. The least squares fit for this data produced a D_a of 30.3 cm^2/s. The computed profiles at D_a = 15.3 cm^2/s and at D_a = 49.3 cm^2/s bound the data, and a profile at the measured value D_a = 30.6 cm^2/s appears (as expected) to be the best correlation.[23]

D. Deduced D_a compared with measurement.

Given (E/N) and N, one can compute D_a, α, and (kT_e/e) for nitrogen. The details of these computations are described in Appendix C. Figure 18 shows a representative vertical (y) profile of D_a (x near the center port, P_0 = 239 kPa). A similar profile for (kT_e/e) appears as Fig. 20.

The plasma in the discharge channel is predominately confined to the lower half of the discharge gap ($y/y_I < 0.5$). In this region, the values of D_a and (kT_e/e) change only slightly. For all experimental conditions considered here, (kT_e/e) was found to lie between 0.65 and

0.75 eV near the cathode. (For D_a values deduced from z-profiles, see Table I.)

Local flow density measurements are the most crucial ones for experimentally determining D_a. D_a varies quite slowly with (E/N), but it is inversely proportional to density N. The scatter associated with the accepted values of drift velocity used to compute D_a is, however, substantially higher than expected errors associated with the uncertainties of the present experiment.

The method of deducing D_a values from experimental z-profile data has been discussed in Sec. V-B-2 above. Deduced D_a values agree very well with measured ones at the same tunnel coordinates. Figure 19, discussed in Sec. V-C, illustrates this agreement for a specific case.

E. Further comparison: x-variation

Measurements show that the maximum plasma density near the rear port is about half the maximum measured at the center port for similar discharge conditions. A computation of the plasma density from theory using Eq. (18) also predicts this x-variation. The computation was performed with typical values of u (540 m/s), D_a (40 cm^2/s), and α (100 to 1000 s^{-1}), and with a 10-point approximation to the line source

$$A(x) = K\,\delta(x - x_0)\,\delta(z - z_0)\,\exp(-Hy)\ ,$$

where K is a constant and $H = 1\ cm^{-1}$. Both results indicate an x-direction variation in plasma density dominated by the (1/r) decay term, rather than by the exponential factor $\exp(\alpha|x - x_0|/u)$. Hence, the vertical distribution of plasma in the discharge channel results from convection of an initial upstream source and not from diffusion or production processes.

The effect of the source on x-direction variation can be demonstrated by examining a centerline ($z = z_0$) location downstream, where $r = (x - x_0) \gg (y - y_0)$. Let the strength of any point (x_0, y, z_0) on the line source along y at (x_0, z_0) be proportional to $\exp(-Hy)$. Each source point will contribute a term like Eq. (19) to the density at any position (x, y, z) farther downstream. If the plasma density at height $y = y_1$ results chiefly from the upstream source point at y_1 and not from line source points flanking y_1, then the (1/r) decay along x dominates $\exp(\alpha|x - x_0|/u)$ in Eq. (19). Consider two arbitrary source points, one at y_1 and one above it at y_2. The ratio of n_1, the plasma density contribution at (x, y_2, z_0) from the source point at (x_0, y_1, z_0), to n_2, the plasma density contribution at (x, y_2, z_0) from the source point at (x_0, y_2, z_0), is approximately

$$\frac{n_1}{n_2} = \exp\left[-\left(\frac{u}{4D_a}\frac{(y_2 - y_1)}{(x - x_0)} - H\right)(y_2 - y_1)\right] \quad . \tag{20}$$

When the exponent in Eq. (20) is small or 0, the plasma density contribution from the source point at (x_0, y_2, z_0) to positions further down the same streamline is comparable to the contribution from the lower source point at (x_0, y_1, z_0). When the exponent is large and negative, the major source of plasma along the (y_2, z_0)-streamline is the upstream source point at (x_0, y_2, z_0).

The exponent in Eq. (20) is 0 when

$$(x - x_0) = (u/4D_a)\,(y_2 - y_1)/H \quad ,$$

and it is negative for smaller $(x - x_0)$. If $u = 540$ m/s, $D_a = 40\text{cm}^2/\text{s}$, and $H = 1\ \text{cm}^{-1}$, then negative exponents occur when

$$(x - x_0) < 350(y_2 - y_1) \quad .$$

So the source point at (x_0, y_1, z_0) will not affect the flow along the (y_2, z_0)-streamline until $350(y_2 - y_1)$ cm downstream. For this reason, only 10% of the line source (a 0.25-cm segment centered on the y_E-streamline) will influence plasma density at a point of height y_E at the discharge volume exit, where $(x - x_0) = 50$ cm. Clearly, convection of the source distribution along x dominates diffusion.

VI. CONCLUSIONS

Experiments were performed with a single electrode probe in a discharge volume. Their goal was to measure relative plasma density profiles in a spatially resolved manner at two locations downstream of a pin discharge for two flow conditions. These data give a direct indication of the extent and distribution of the plasma in the discharge volume. The horizontal (z) profiles of the plasma plume behind one pin look much like the swept conical clouds predicted by the theory of Sec. III. The vertical (y) profile, however, requires an assumption of a line source of variable strength. The data gathered can be evaluated by fitting Gaussians in $(z - z_0)$ to horizontal data profiles; in this manner, values of the ambipolar diffusion coefficient can be deduced. The theory reproduces observed x-variations in plasma density for the values of D_a and u found by experiment.

Near the cathode, where the majority of the plasma is located, D_a values derived from experiment correlate quite well with those computed from (E/N) and N data. In this region, D_a is nearly constant and u does not vary too drastically, thus approximating the assumptions of the theory of Sec. III. This theory, therefore, provides a concise description of the general features of the plasma flow in the double discharge.

ACKNOWLEDGMENTS

The author would like to acknowledge the concern, assistance, and involvement of his thesis advisor, Professor George K. Bienkowski, throughout his graduate research. To Roy Woodruff and T. R. Girill the author is also grateful, for their part in seeing this paper to completion. This work was performed under the auspices of the U.S. Department of Energy by Lawrence Livermore Laboratory under contract No. W-7405-Eng-48, and in part by AFOSR under contract No. F44620-73-C-0059.

APPENDIX A: APPARATUS

The nozzle of the discharge device used in this study has a nominal Mach number of 3.93, and an area ratio of 10.08. Its length from throat to parallel plates is 19.69 cm. Behind the nozzle lies the discharge volume, whose physical features are summarized in Table II.

The pin electrodes are placed in the tunnel floor so that the first row of pins lies 1.27 cm from the cathode's leading edge. The next four rows are 2.54 cm apart, while the sixth and seventh rows are spaced at 7.62-cm intervals. The center pin of each row lies on the tunnel centerline; the others are at 1.27-cm intervals on either side. Table III gives details on the construction of these electrodes.

The flush-mounted glass windows are located midway between the cathode and anode at 5.08, 25.40, and 45.72 cm from the leading edge of the discharge volume. Each is 4.64 cm in diameter, giving a full view of the discharge gap.

APPENDIX B: RELATIONSHIP BETWEEN I_{rms} and I_{SAT}

The definition of the rms value is

$$V_{rms}^2 = (f/2\pi) \int_0^{2\pi/f} V^2(ft)\, dt \quad ,$$

where f is frequency.

Because the peak of the voltage signal sent into the plasma is significantly larger than (kT_e/e), a saturation current will be achieved quickly in any half cycle, and will be maintained throughout the majority of that half cycle. Thus the expected current signal across a test resistor is an asymmetric square wave with peaks of value $|I_{eSAT}|$ and $|I_{+SAT}|$. For such a signal,

$$I_{rms} = (1/\sqrt{2})\left(I_{+SAT}^2 + I_{eSAT}^2\right)^{\frac{1}{2}}$$

$$= (1/\sqrt{2})\left[1 + \left(I_{eSAT}/I_{+SAT}\right)^2\right]^{\frac{1}{2}} I_{+SAT} \quad .$$

From the approximations used in studying the probe response, the ratio of saturation currents was found to be

$$|I_{eSAT}/I_{+SAT}| = (\mu_e/\mu_+) \approx (m_+/m_e)^{\frac{1}{2}} \quad .$$

Therefore,

$$I_{rms} = I_{+SAT}\ (1/\sqrt{2})\left(1 + (m_+/m_e)\ \right)^{\frac{1}{2}}$$

$$= I_{+SAT}\ (m_+/2m_e)^{\frac{1}{2}} \quad ,$$

so that

$$I_{+SAT} = (2m_e/m_+)^{\frac{1}{2}}\ I_{rms} \quad .$$

APPENDIX C: FORM OF D_a IN SLIGHTLY IONIZED GAS

We know from Sec. III-B that

$$D_a = \frac{D_+ + (\mu_+/\mu_e)\, D_e}{1 + (\mu_+/\mu_e)} \quad ,$$

where

$$(\mu_+/\mu_e) \approx (m_e/m_+)^{\frac{1}{2}} << 1 \quad .$$

Hence

$$D_a \approx D_+ + (\mu_+/\mu_e)\, D_e \quad .$$

The ratio of D_s/μ_s is a characteristic or average energy of particles in species s, so that

$$(D_e/\mu_e) = (2\varepsilon/3) = (kT_e\ /e) \quad .$$

This is called the Einstein relation in equilibrium situations where T_e is constant; here, T_e is a <u>defined</u> temperature and ε is the average electron energy locally. Substitution yields

$$D_a \approx D_+ + \mu_+\ (kT_e/e)$$

$$\approx \mu_+ \left[\frac{D_+}{\mu_+} + \frac{kT_e}{e}\right] .$$

Because the ions are cold, they are assumed to be in equilibrium at a temperature $T_+ \approx T$. Consequently,

$$D_a \approx \mu_+ \left[\frac{kT_+}{e} + \frac{kT_e}{e} \right] \quad .$$

By the definition of cold ions, $T_+ << T_e$, which means that

$$D_a \approx (kT_e/e)\ \mu_+ \quad .$$

The ambipolar diffusion coefficient is therefore the product of two-thirds the average electron energy and the ionic mobility coefficient.

A relationship between the ionic drift velocity and (E/N) has also been assumed, using drift velocity data in nitrogen taken from McDaniel.[24] The equation used for μ_+ is

$$\mu_+ = \frac{(10^4/N)}{28C + (E/N)} \left\{ \frac{28}{6.4} + 45 \left[\frac{(E/N)}{1000C} \right]^{0.615} \right\} \quad ,$$

where μ_+ is in $cm^2/V \cdot s$ and $C = 3.11 \times 10^{-17}\ V \cdot cm^2$. The drift velocity is simply $\underset{\sim}{v}_+ = \mu_+ \underset{\sim}{E}$, which is a function solely of (E/N).

Based on computations of electron energy distribution functions, Nighan[25] has produced a plot of (kT_e/e) vs (E/N). A fit made to this plot and used subsequently in this paper is

$$(kT_e/e) = \frac{(0.153 \log (E/N)) + 3.090}{1 + \exp\left[\frac{10}{3}\left(\frac{E}{N}\, 10^{16} - 8\right)\right]} + \frac{(4.800 \log (E/N) + 73.485) \exp\left[\frac{6}{5}\left(\frac{E}{N}\, 10^{16} - 7\right)\right]}{1 + \exp\left[\frac{6}{5}\left(\frac{E}{N}\, 10^{16} - 7\right)\right]} .$$

This equation governs N_2 gas, where the units for (kT_e/e) and for (E/N) are eV and $V \cdot cm^2$, respectively.

Nighan and Wiegand[26] have also produced a plot of ionization rate coefficient α against (kT_e/e). A fit made to this curve and used hereafter is $\log (\alpha/N) = -14.427\ (kT_e/e)^{-0.368}$, where α is in s^{-1}, N is in cm^{-3}, and (kT_e/e) is in eV.

[a] Research was conducted at the Department of Aerospace and Mechanical Sciences (now Mechanical and Aerospace Engineering), Princeton University.

[1] W. L. Nighan, Phys. Rev. A 2, 1984 (1970).

[2] W. L. Nighan, Appl. Phys. Lett. 20, 96 (1972).

[3] C. K. N. Patel, and R.J. Keel, Appl. Phys. Lett. 5, 81 (1964).

[4] C. K. N. Patel, Phys. Rev. 141, 71 (1966).

[5] J. P. Reilly, Astronautics and Aeronautics 13, 52 (1975).

[6] T. G. Jones, S. R. Bryon, A. L. Hoffman, B. B. O'Brien, and W. B. Lacina, "Electron-Beam Stabilized CW Electric Discharge Laser in Supersonically Cooled $CO/N_2/Ar$ Mixtures," AIAA 7th Fluid and Plasma Dynamics Conference, Palo Alto, Calif., June 1974 (AIAA paper No. 74-562).

[7] J. H. Blom, and R. K. Hanson, Appl. Phys. Lett. 23, 190 (1975).

[8] M. Garcia, "A Study of an Electric Discharge in a Supersonic Nitrogen Stream," Ph.D. Thesis 1374-T, Department of Aerospace and Mechanical Sciences (now Mechanical and Aerospace Engineering), Princeton University, May 1978. Available from University Microfilms, No. 78-18336.

[9] I. P. French, R. A. Hayami, T. E. Arnold, M. Steinberg, J. P. Appleton, and A. A. Sonin, AIAA J. 8, 2207 (1970).

[10] R. A. Haas, Phys. Rev. A 8, 1017 (1973).

[11]W. P. Allis, Physica 82C, 43-51 (1976).

[12]W. L. Nighan, and W. J. Wiegand, The Gaseous Electronics of Lasers (John Wiley, New York, 1976). Also quoted in W. P. Allis, Physica 82C, 43-51 (1976).

[13]N_2 Second Positive System Emission.

[14]N_2 First Positive System Emission.

[15]E. W. McDaniel, Collision Phenomena in Ionized Gases (John Wiley & Sons, New York, 1964), p. 381.

[16]E. W. McDaniel, Ref. 15, p. 373.

[17]S. H. Lam, "Compressibility and Nonequilibrium Effects on the Response of a Langmuir-Probe in a Flowing Plasma," AIAA Paper 65-543, San Francisco, Calif., July 1965.

[18]E. W. McDaniel, Ref. 15, p. 353.

[19]Which is of the order of 10^{-17} cm^3/s. See D. H. Douglas-Hamilton, J. Chem. Phys. 58, 4820 (1973).

[20]Reference to a company or product name does not imply approval or recommendation of the product by the University of California or the U.S. Department of Energy to the exclusion of others that may be suitable.

[21]One can estimate plasma density in cm^{-3} by multiplying the data displayed as $(V_{rms}$ - noise)/0.5 V by 1.7×10^{10} when P_0 = 239 kPa, and by 8.5×10^9 when P_0 = 120 kPa.

[22]This condition was chosen because it was easier to produce a good match with experimental observations. Whether the actual quasi-neutral boundary condition at the plate surface is zero gradient or zero (that is, extremely small) value, the region in which this boundary condition would affect the plasma density contours is below the reach of experiment.

[23]For z-profiles, the fit to experimental points by Gaussian curves resulted in a goodness-of-fit parameter r usually better than 0.9 (r = 1.0 signifies a perfect fit).

[24]E. W. McDaniel, Ref. 15, p. 476.

[25]W. L. Nighan, Phys. Rev. A 2, 1994, Fig. 6 (1970).

[26]W. L. Nighan, and W. J. Wiegand, Phys. Rev. A 10, 925, Fig. 1 (1974).

NOTICE

"This report was prepared as an account of work sponsored by the United States Government. Neither the United States nor the United States Energy Research & Development Administration, nor any of their employees, nor any of their contractors, subcontractors, or their employees, makes any warranty, express or implied, or assumes any legal liability or responsibility for the accuracy, completeness or usefulness of any information, apparatus, product or process disclosed, or represents that its use would not infringe privately-owned rights."

TRG/rls

TABLE CAPTIONS

TABLE I. D_a deduced from z-profiles for measured u values at two port locations.

TABLE II. Discharge volume dimensions.

TABLE III. Electrode construction.

TABLE I. D_a deduced from z-profiles for measured u values at two port locations.

P_o (kPa)	y/y_I	u (m/s)		D_a (cm^2/s)	
		Center	Rear	Center	Rear
239	0.05	433	466	19.39-26.08; 30.29	28.30-40.24
	0.07	444	464	20.03	
	0.10	459	481		22.79
	0.15	467	503	30.33-34.49	33.63
	0.20	470	513		36.31
	0.27	482	522	71.80	63.04
	0.35	520	534	98.67-121.65	85.33
	0.43	570	549	135.05	
	0.50	605	551	158.15-266.32	
120	0.07	444	464	55.34-72.04	50.89-48.59
	0.10	459	481	62.45-128.76	
	0.27	482	522		105.80
	0.50	605	551		184.33
	0.54	612	556	139.58-269.89	

TABLE II. Discharge volume dimensions.

Position	Reference Length (from throat)	Height cm	Width cm	Area cm^2
throat	0	2.54	0.635	1.61
leading edge	21.90	2.55	6.40	16.31
trailing edge	72.71	2.93	6.40	18.76

TABLE III. Electrode construction.

Item	Geometry	Materials
discharge plates	50.80 cm, span full width, rounded leading & trailing edges, latter exposed	copper
pins	0.0635-cm diam, flush with cathode surface, 7 rows of 5 across	tungsten
insulators	0.2381-cm diam, flush with cathode surface	boron nitride

FIGURE CAPTIONS

FIG. 1. Inverted view of the supersonic electric discharge device.

FIG. 2. Plasma behavior between the double discharge plates. (The plate separation at the entrance to the discharge volume is $y_I = 2.54$ cm.)

FIG. 3. General circuit diagram of the double discharge.

FIG. 4. Normalized flow velocity vs y/y_I at the center port ($P_0 = 239$ kPa, $y_I = 2.54$ cm, $u_{peak} = 612.43$ m/s).

FIG. 5 Normalized neutral density vs y/y_I at the center port ($P_0 = 239$ kPa, $y_I = 2.54$ cm, $N_{peak} = 1.54 \times 10^{18}$ cm^{-3}).

FIG. 6. Voltage-current characteristics for several pin currents I_0 ($P_0 = 207$ kPa). A marks observed arcing onset.

FIG. 7. Constant density surfaces for semi-infinite solution of Eq. (18).

FIG. 8. Circuit for plasma density and floating potential probe.

FIG. 9. Normalized probe signal vs distance along y-axis at center port ($P_0 = 239$ kPa, $I_0 = 1$ A dc, $I = 0.5$ A dc).

FIG. 10. Normalized probe signal vs horizontal position at six vertical distances (1 through 6) from the cathode. Excursion bars suppressed.

FIG. 11. Constant plasma density contours (normalized by peak probe signal at the center port). Height from cathode vs horizontal location. Circles indicate the horizontal scan locations used in FIG. 8. Excursion bars suppressed.

FIG. 12. Normalized probe signal vs distance along y-axis at rear port (P_0 = 239 kPa, I_0 = 1 A dc, I = 0.5 A dc).

FIG. 13. Normalized probe signal vs horizontal position at rear port (y = 0.28 cm, P_0 = 239 kPa, I_0 = 1 A dc, I = 0.5 A dc, tunnel width z_T = 6.4 cm).

FIG. 14. Floating potential vs y/y_I at center port (P_0 = 239 kPa, I_0 = 1 A dc, I = 0.5 A dc, y_I = 2.54 cm).

FIG. 15. (E/N) vs y/y_I at the center port (P_0 = 239 kPa, I_0 = 1 A dc, I = 0.5 A dc).

FIG. 16. Normalized plasma density vs vertical position y at the center port (P_0 about 239 kPa, (E/N) = 2.56×10^{-16} V•cm^2, N = 8.93×10^{17} cm^{-3}, D_a = 46.9 cm^2/s).

FIG. 17. Normalized plasma density vs horizontal position (z/z_T) at the center port (P_0 about 239 kPa, (E/N) = 2.56×10^{-16} V•cm^2, N = 8.93×10^{17} cm^{-3}, D_a = 46.9 cm^2/s).

FIG. 18. Ambipolar diffusion coefficient D_a vs vertical position (y/y_I) at the center port (P_0 = 239 kPa, I_0 = 1 A dc, I = 0.5 A dc).

FIG. 19. Theoretical normalized plasma density profiles compared with normalized experimental data at the center port. Squares are data points reflected about $(z/z_T) = 0.5$. Extent of horizontal bars equals (probe diameter)/z_T. (P_0 = 239 kPa, I_0 = 1 A dc, I = 0.5 A dc, $y/y_I = 0.05$).

FIG. 20. Energy (kT_e/e) vs vertical position (y/y_I) at the center port (P_0 = 239 kPa, I_0 = 1 A dc, I = 0.5 A dc).

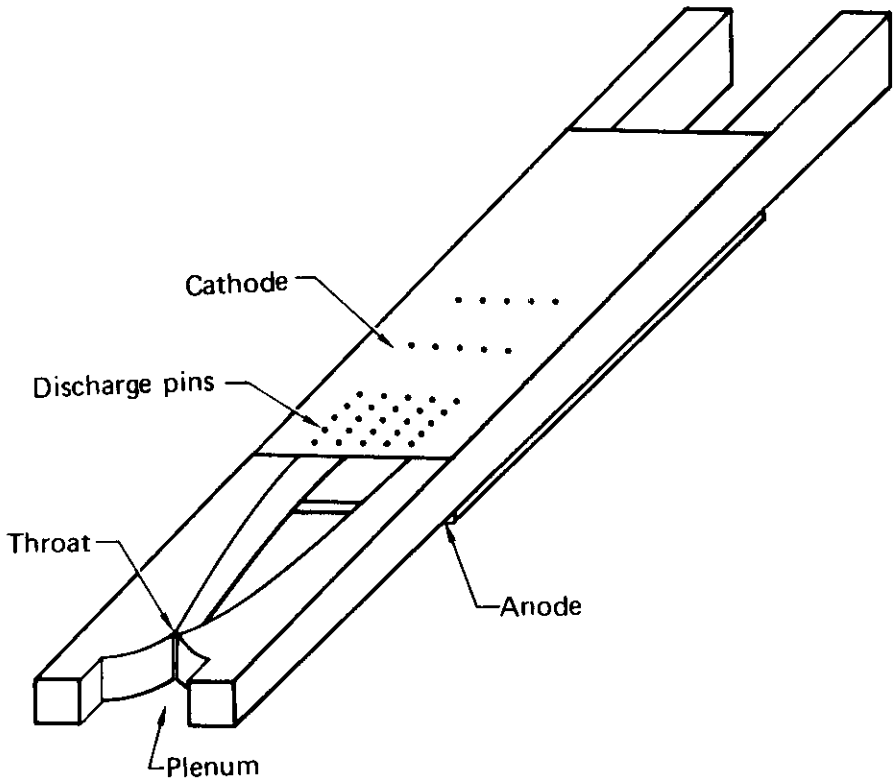

Garcia - Fig. 1

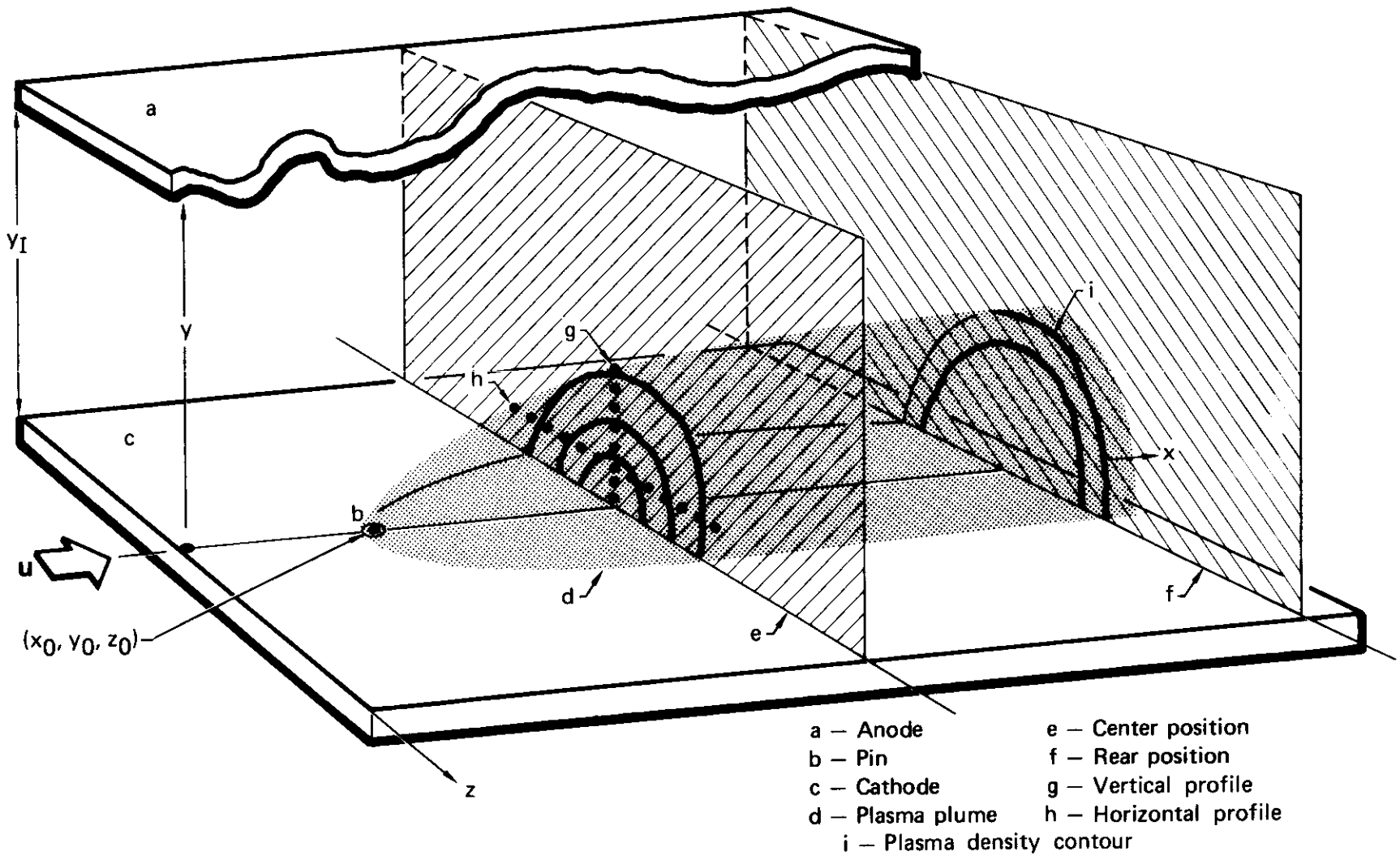
a
y_I
y
c
b
u
(x_0, y_0, z_0)
g
h
i
x
d
e
f
z
a — Anode
b — Pin
c — Cathode
d — Plasma plume
e — Center position
f — Rear position
g — Vertical profile
h — Horizontal profile
i — Plasma density contour

Garcia - Fig. 2

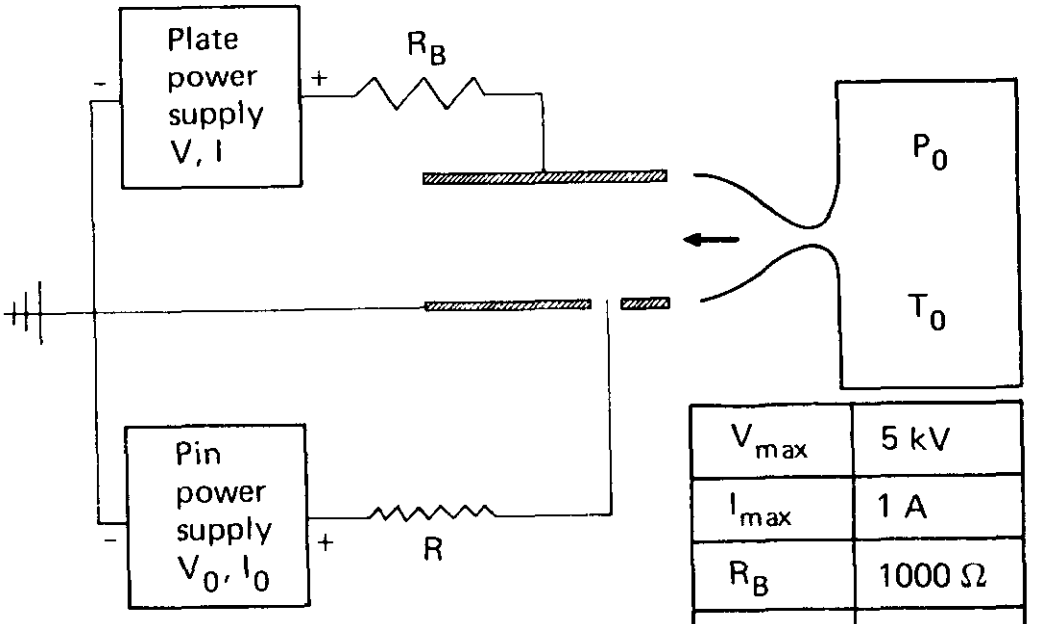

V_{max}	5 kV
I_{max}	1 A
R_B	1000 Ω
$V_{0_{max}}$	1.25 kV
$I_{0_{max}}$	2.5 A
R	3000 Ω

Garcia - Fig. 3

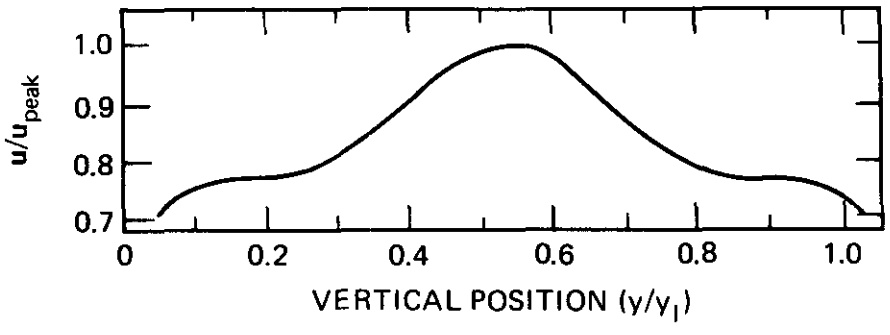

Garcia - Fig. 4

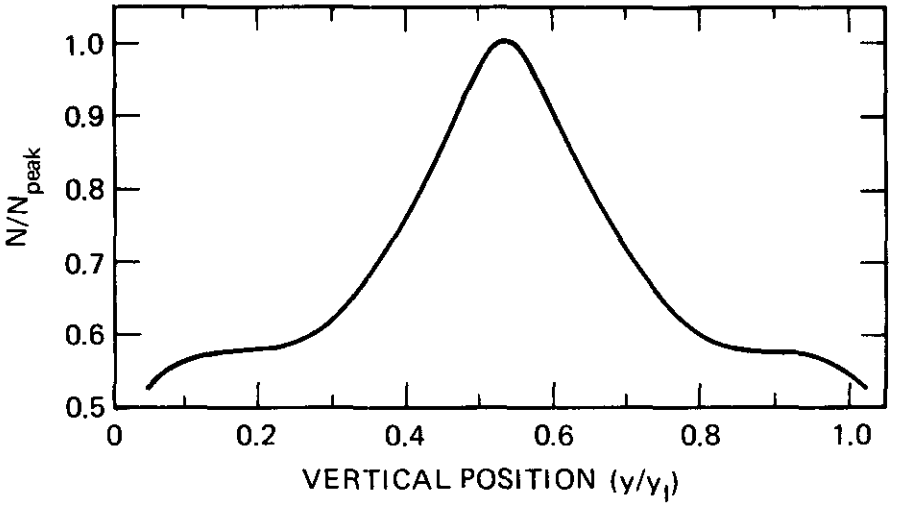

Garcia - Fig. 5

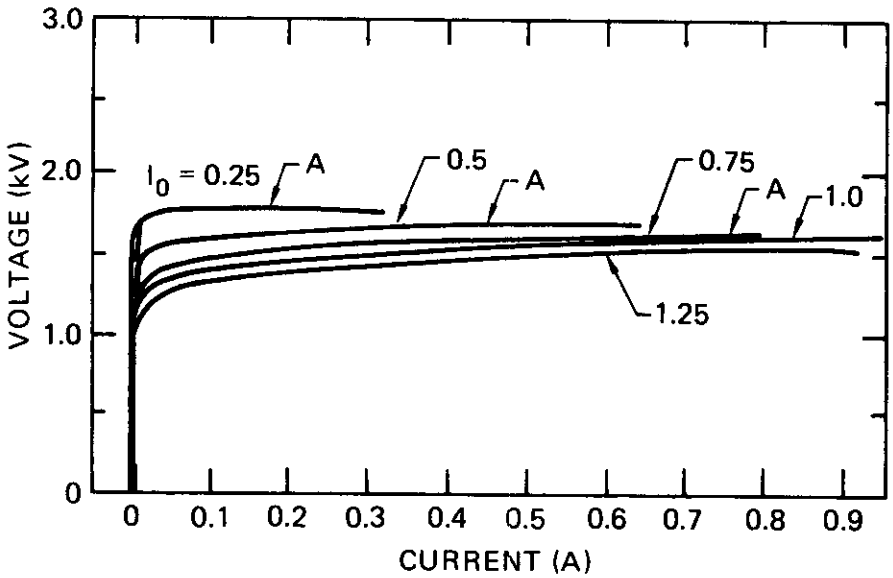
3.0
2.0
1.0
0
VOLTAGE (kV)
I_0 = 0.25 A
0.5 A
0.75 A
1.0
1.25
0
0.1
0.2
0.3
0.4
0.5
0.6
0.7
0.8
0.9
CURRENT (A)

Garcia - Fig. 6

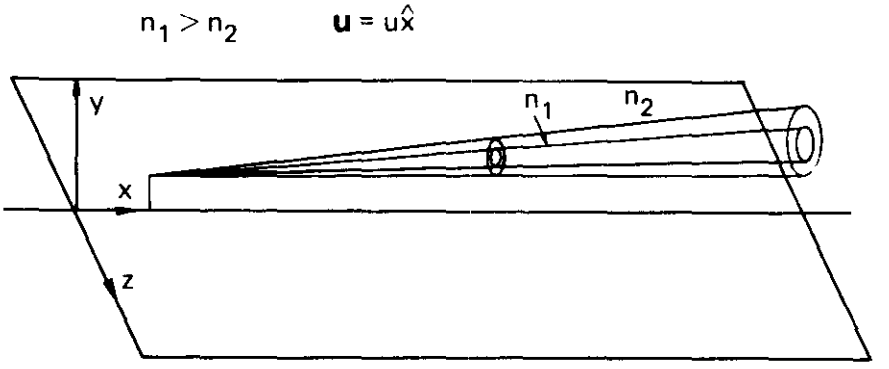

Garcia - Fig. 7

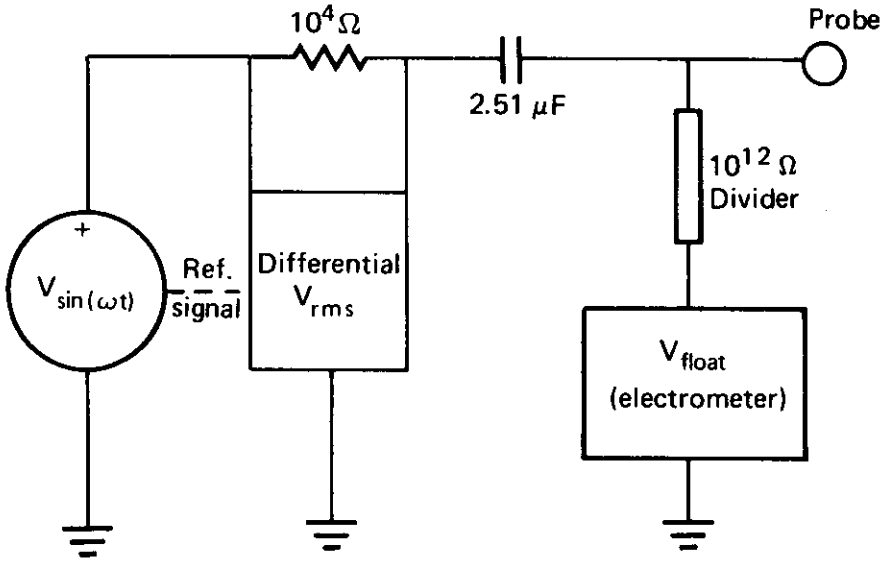
$10^4\,\Omega$
Probe
2.51 μF
$10^{12}\,\Omega$
Divider
+
$V_{\sin(\omega t)}$
Ref.
signal
Differential
V_{rms}
V_{float}
(electrometer)

Garcia - Fig. 8

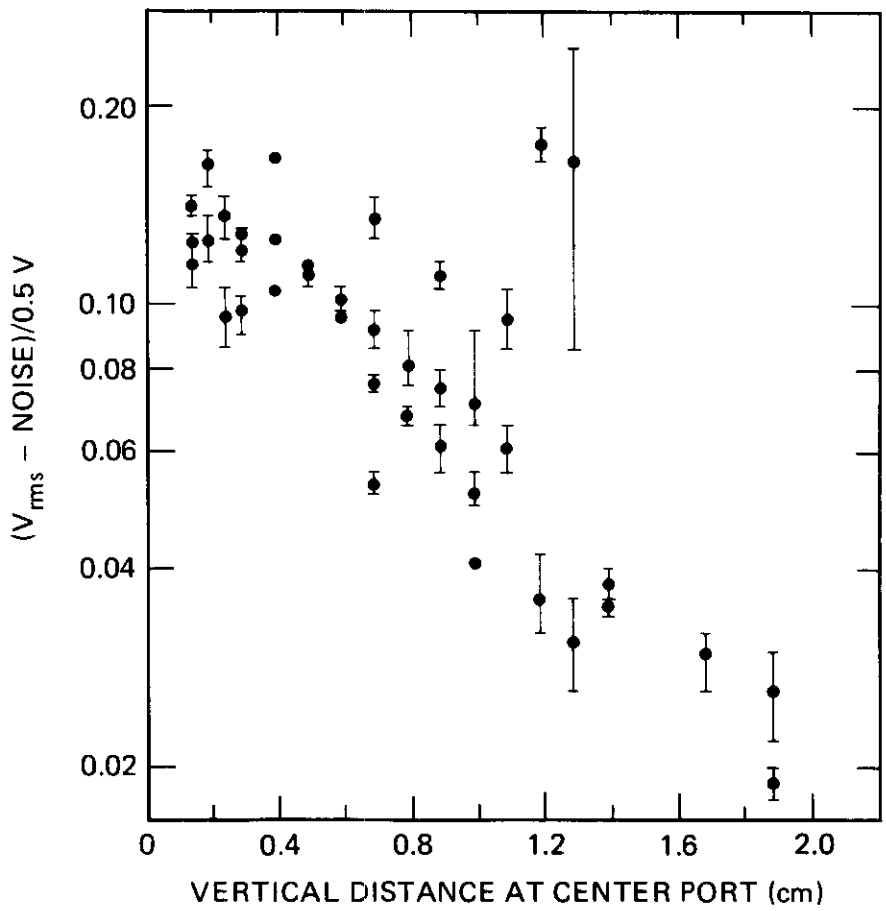
0.20
0.10
0.08
0.06
0.04
0.02
$(V_{rms}$ – NOISE)/0.5 V
0
0.4
0.8
1.2
1.6
2.0
VERTICAL DISTANCE AT CENTER PORT (cm)

Garcia - Fig. 9

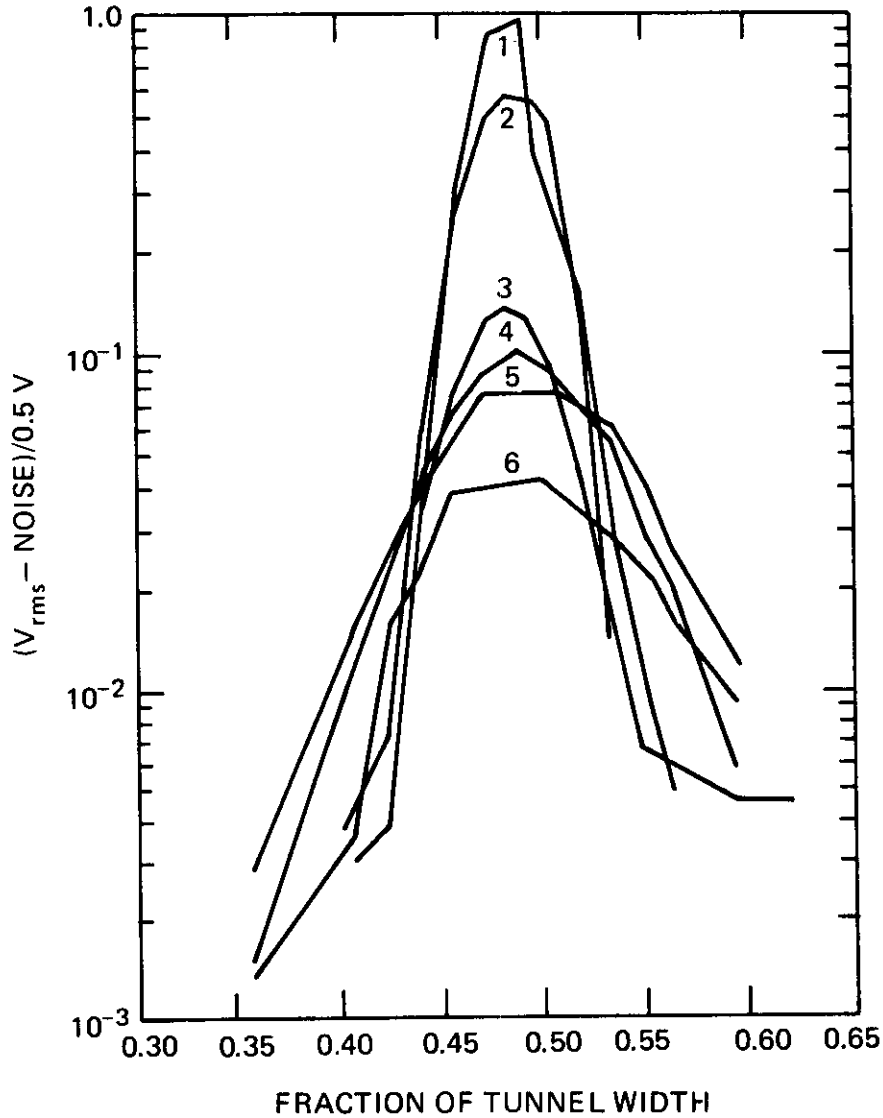

Garcia - Fig. 10

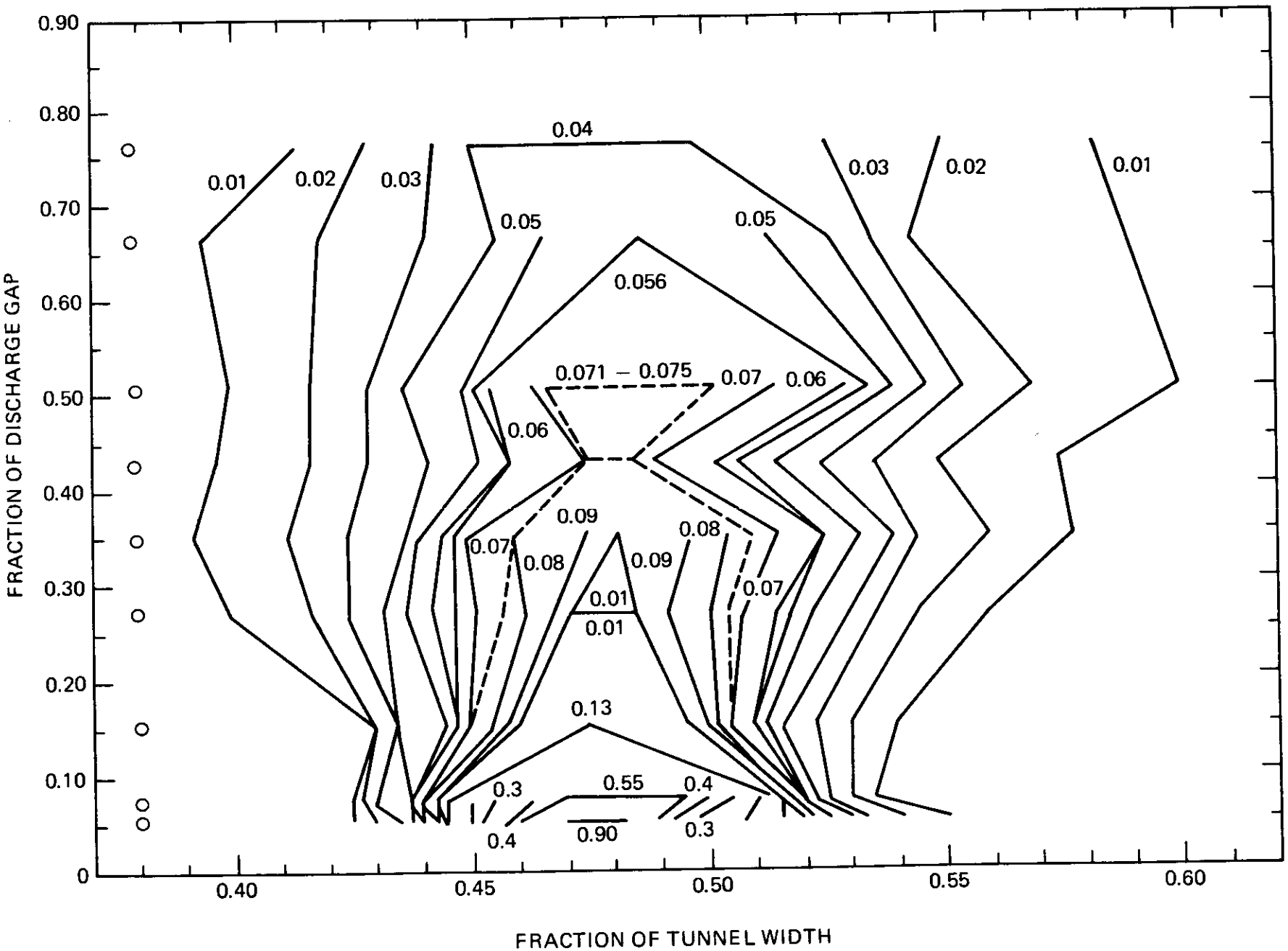

Garcia - Fig. 11

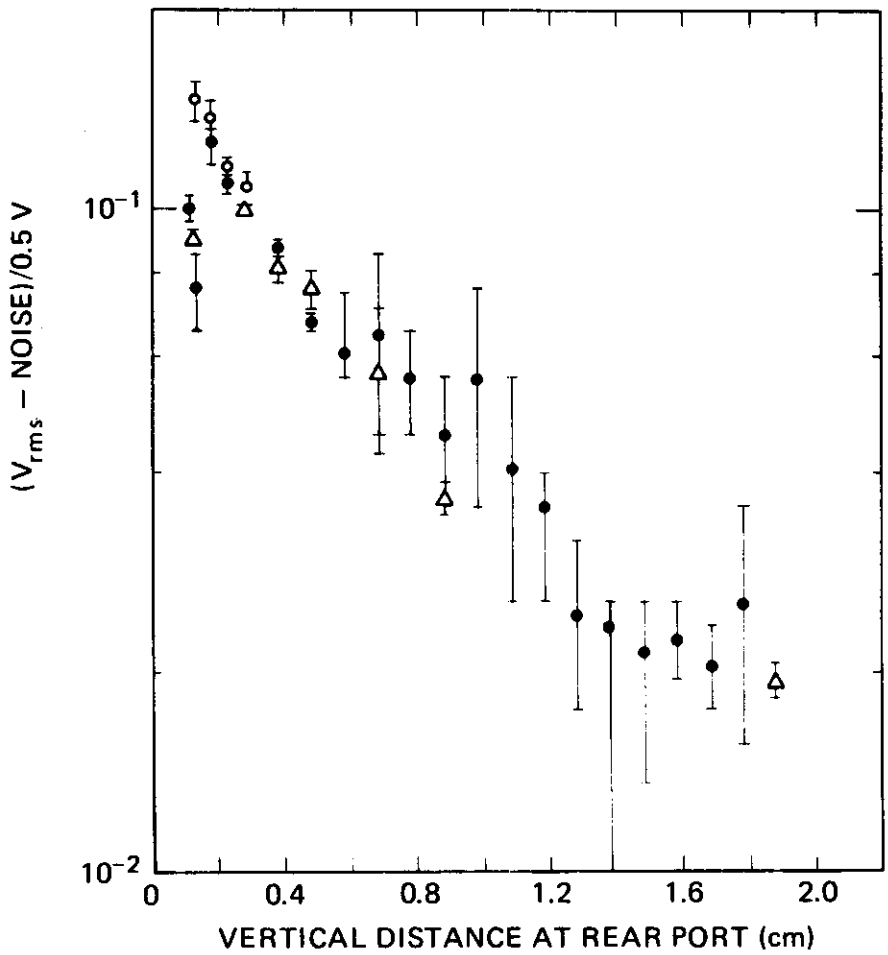

Garcia - Fig. 12

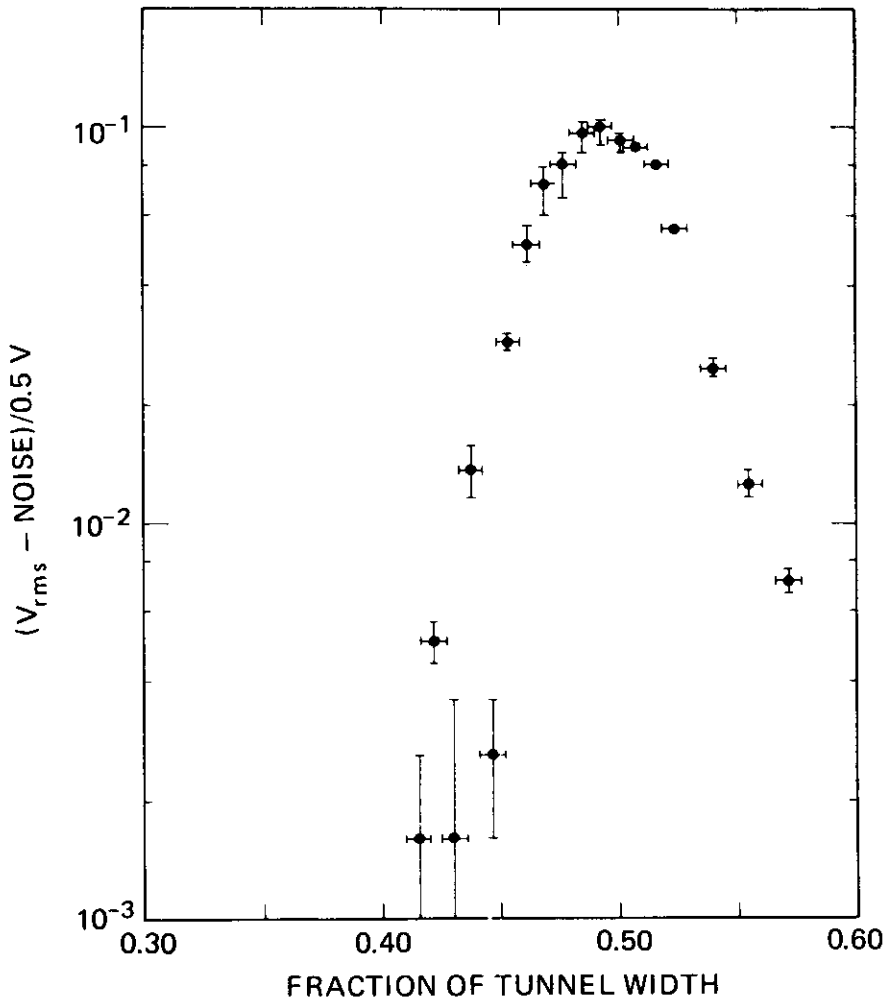

Garcia - Fig. 13

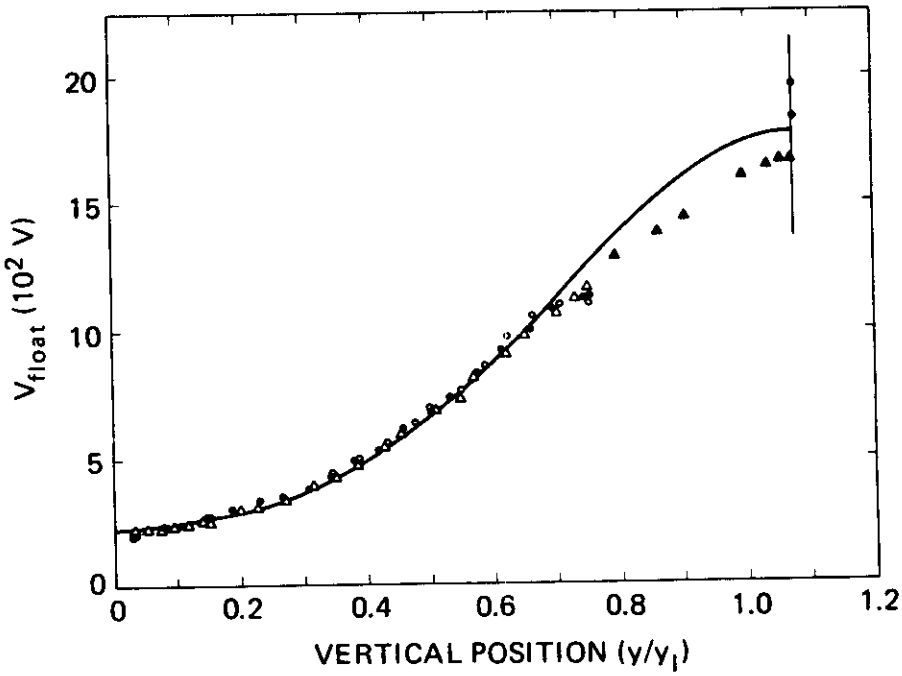

Garcia - Fig. 14

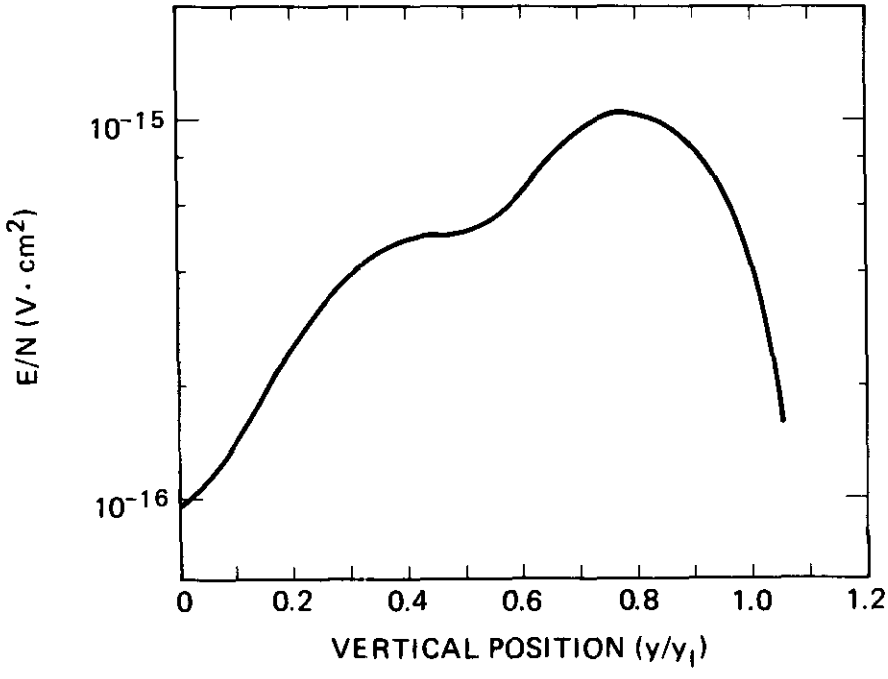

Garcia - Fig. 15

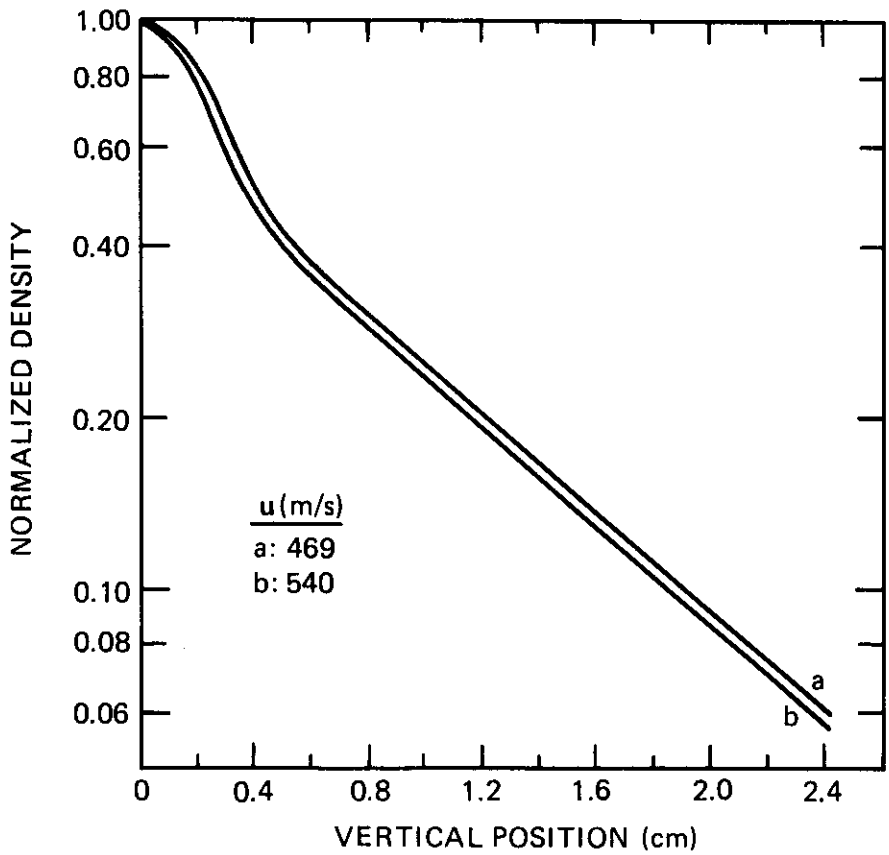

Garcia - Fig. 16

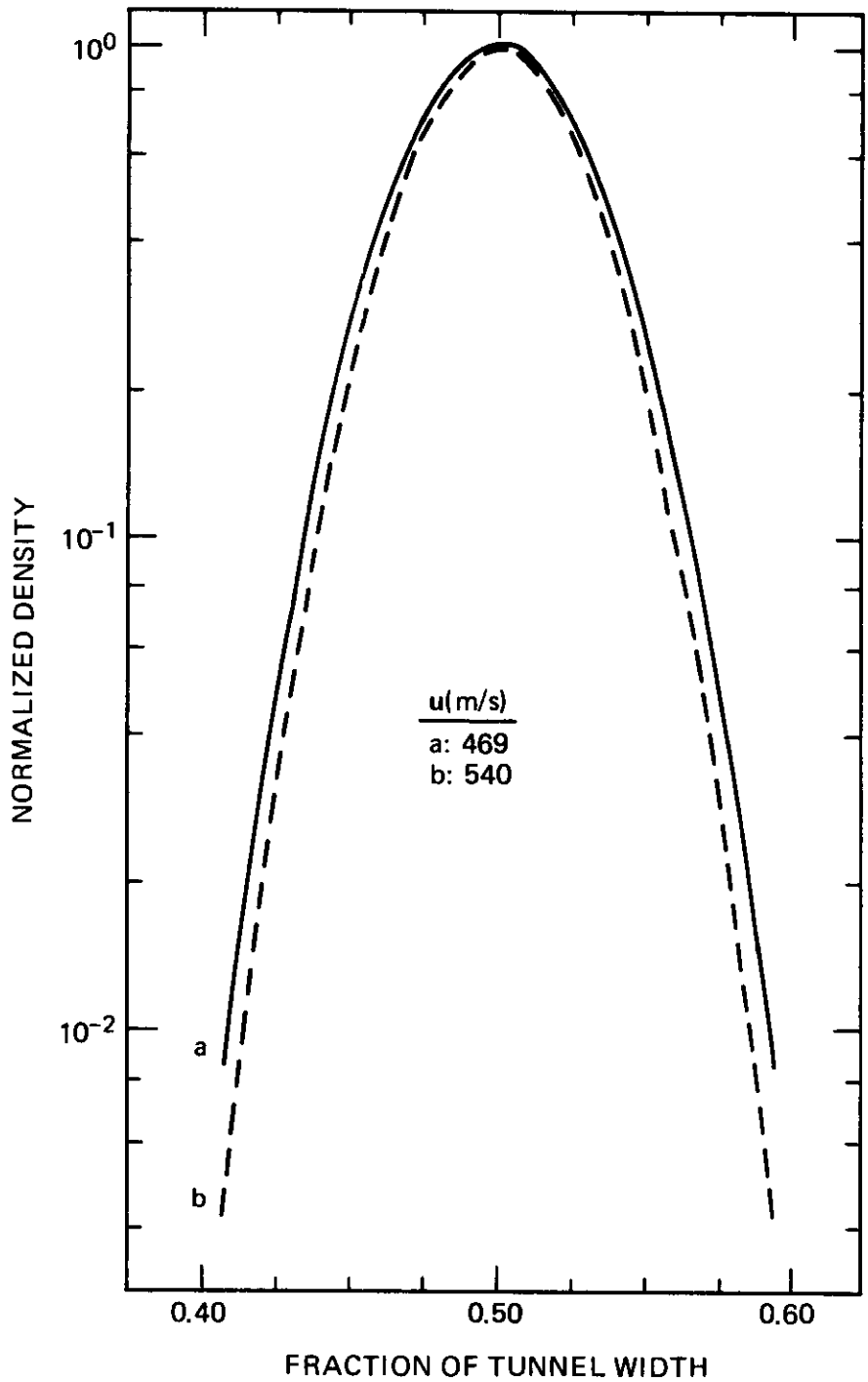

Garcia - Fig. 17

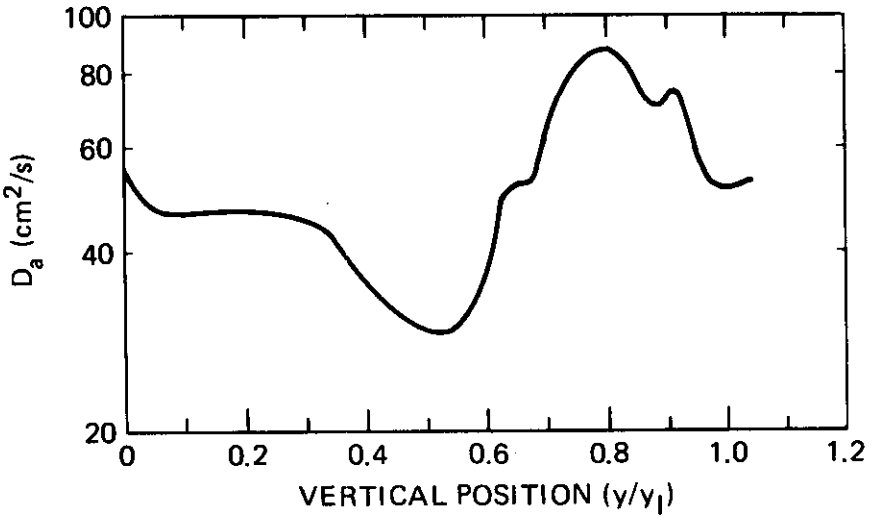

Garcia - Fig. 18

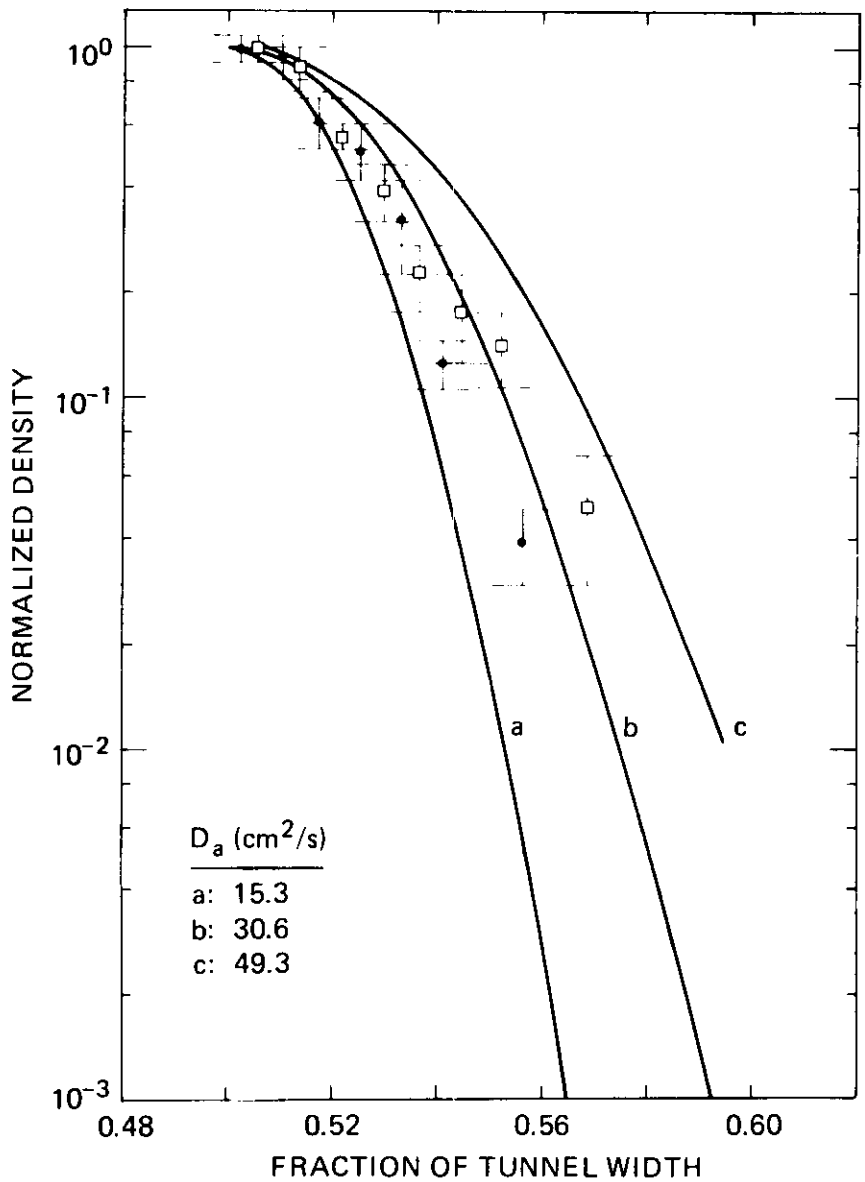

Garcia - Fig. 19

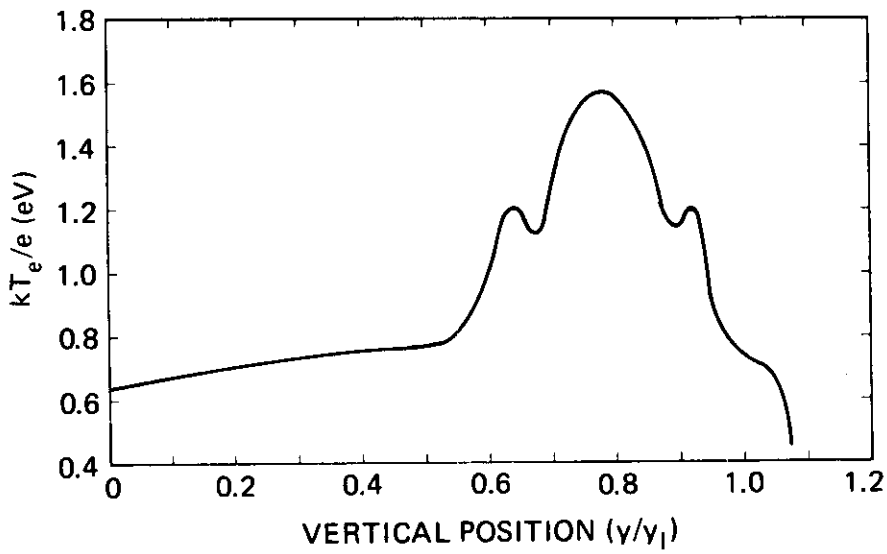

Garcia - Fig. 20